JCB Journal of Cell Biology

ARTICLE

Noncanonical regulation of phosphatidylserine metabolism by a Sec14-like protein and a lipid kinase

Yaxi Wang[1,2], Peihua Yuan[2], Aby Grabon[2], Ashutosh Tripathi[2], Dongju Lee[2], Martin Rodriguez[1], Max Lönnfors[2], Michal Eisenberg-Bord[3], Zehua Wang[4,5], Sin Man Lam[5], Maya Schuldiner[3], and Vytas A. Bankaitis[1,2,6]

The yeast phosphatidylserine (PtdSer) decarboxylase Psd2 is proposed to engage in a membrane contact site (MCS) for PtdSer decarboxylation to phosphatidylethanolamine (PtdEtn). This proposed MCS harbors Psd2, the Sec14-like phosphatidylinositol transfer protein (PITP) Sfh4, the Stt4 phosphatidylinositol (PtdIns) 4-OH kinase, the Scs2 tether, and an uncharacterized protein. We report that, of these components, only Sfh4 and Stt4 regulate Psd2 activity in vivo. They do so via distinct mechanisms. Sfh4 operates via a mechanism for which its PtdIns-transfer activity is dispensable but requires an Sfh4-Psd2 physical interaction. The other requires Stt4-mediated production of PtdIns-4-phosphate (PtdIns4*P*), where Stt4 (along with the Sac1 PtdIns4*P* phosphatase and endoplasmic reticulum–plasma membrane tethers) indirectly modulate Psd2 activity via a PtdIns4*P* homeostatic mechanism that influences PtdSer accessibility to Psd2. These results identify an example in which the biological function of a Sec14-like PITP is cleanly uncoupled from its canonical in vitro PtdIns-transfer activity and challenge popular functional assumptions regarding lipid-transfer protein involvements in MCS function.

Introduction

The high degree of biochemical compartmentation of eukaryotic cells affords distinct intracellular organelles the capacity to house unique biological functions. This feature is also an isolating principle that demands cells navigate problems associated with execution of physiologically coherent programs of interorganellar communication and signaling that are critical for proper cell homeostasis. Whereas the vesicular pathway that connects organelles of the secretory pathway represents one mechanism by which lipids and proteins traffic between compartments, other evidence supports involvements for nonvesicular modes of lipid trafficking as well. That evidence includes early studies of nonvesicular trafficking of phosphatidylserine (PtdSer) to mitochondria, which were predicated on the assumption that mitochondria represent the sole compartments of residence for the enzyme that decarboxylates PtdSer to phosphatidylethanolamine (PtdEtn). It is now understood that even yeast express two PtdSer decarboxylases: the mitochondrial Psd1 and the endosomal Psd2 (Clancey et al., 1993; Trotter et al., 1993; Trotter and Voelker, 1995). Both enzymes are posited to use membrane contact sites (MCSs) for supply of ER-synthesized PtdSer to the compartments of decarboxylation (Voelker, 2005).

MCSs are actively maintained foci of close apposition between two distinct organelles, and they seemingly bridge essentially all cellular compartments (Shai et al., 2018; Valm et al., 2017; Wu et al., 2018). Characterization of molecules that populate various MCS complexes defines an active research area in contemporary cell biology. More than 20 such MCS classes have been identified, and specific protein components are assigned to each, including lipid transfer proteins and molecular tethers (Levine and Loewen, 2006; Raychaudhuri and Prinz, 2010; Scorrano et al., 2019; Wu et al., 2018). MCS/lipid trafficking models are conceptually attractive, and there is intense speculation regarding how such complexes control lipid flow between organelles. Direct evidence to that effect remains elusive. Ablation of any single MCS component is often without biological consequence. Multiple MCS genes need to be ablated before a phenotype is recognized. Further complicating functional analyses, protein tethers often associate with several MCS classes.

Given that PtdEtn is an essential yeast lipid, mutants defective in both Psd1 and Psd2 activities are Etn auxotrophs (Fig. 1 A). This biological phenotype offers experimental advantages that recommend the yeast PtdSer decarboxylation system as a

[1]Department of Biochemistry and Biophysics, Texas A&M University, College Station, TX; [2]Department of Molecular & Cellular Medicine, Texas A&M Health Science Center, College Station, TX; [3]Department of Molecular Genetics, Weizmann Institute of Science, Rehovot, Israel; [4]University of Chinese Academy of Sciences, Beijing, China; [5]State Key Laboratory of Molecular Developmental Biology, Institute of Genetics and Developmental Biology, Chinese Academy of Sciences, Beijing, China; [6]Department of Chemistry, Texas A&M University, College Station, TX.

Correspondence to Vytas A. Bankaitis: vytas@tamu.edu.

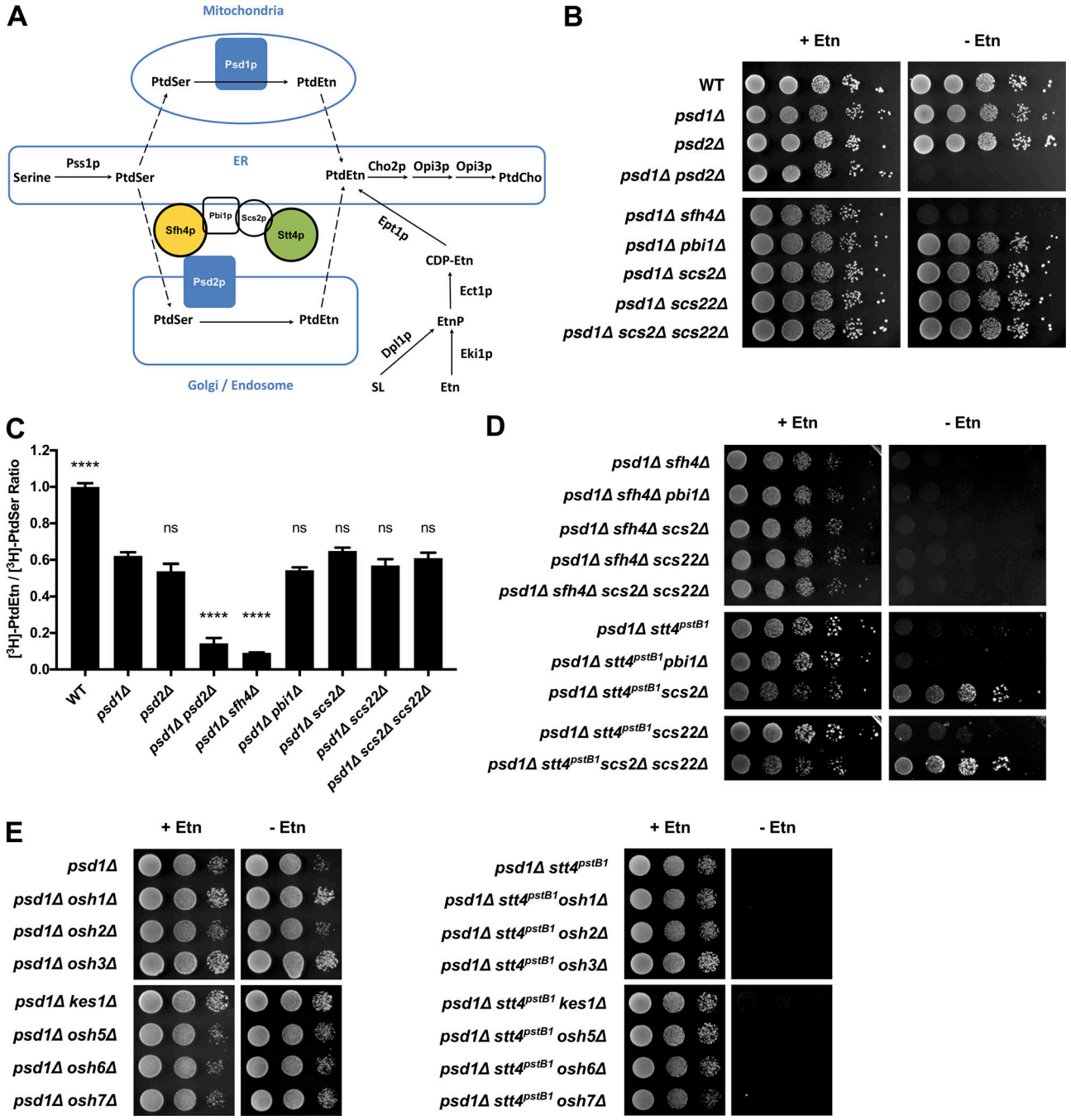

Figure 1. **PtdSer decarboxylation and functional characterization of the Psd2 MCS. (A)** PtdEtn synthesis in yeast occurs via two primary mechanisms. The first involves the decarboxylation of PtdSer catalyzed by either the mitochondrial PtdSer decarboxylase Psd1 or the trans-Golgi network/endosomal-localized PtdSer decarboxylase Psd2. Psd2 activity is proposed to require the assembly of an MCS composed of the Sfh4 PITP, the PtdIns-4-OH kinase Stt4, the molecular tether Scs2 that binds Stt4, and the uncharacterized Pbi1. The second major pathway for PtdEtn synthesis involves salvage of exogenous Etn, or Etn-P produced in the terminal step of sphingolipid degradation, via the action of the cytidine diphosphate (CDP)-Etn pathway. **(B)** Yeast strains of the indicated genotype (at left) were dilution spotted onto solid glucose minimal medium either supplemented with Etn (2 mM) or not as indicated at top. Results were recorded after 72 h of incubation. Failure to grow in the absence of Etn identifies failure in Psd2 pathway activity. **(C)** The efficiencies of PtdSer decarboxylation to PtdEtn were measured for WT, *psd1Δ*, *psd2Δ*, *psd1Δ psd2Δ*, *psd1Δ sfh4Δ*, *psd1Δ pbi1Δ*, *psd1Δ scs2Δ*, *psd1Δ scs22Δ*, and *psd1Δ scs2Δ scs22Δ* strains by radiolabeling cells with [^{3}H]-serine, extraction of total phospholipid, and quantification of [^{3}H]-PtdSer and [^{3}H]-PtdEtn (see Materials and methods). Decarboxylation of PtdSer to PtdEtn was expressed as a [^{3}H]-PtdEtn/[^{3}H]-PtdSer ratio for the indicated strains and related to the [^{3}H]-PtdEtn/[^{3}H]-PtdSer ratio of the WT control (set as 1.0). Values represent averages from three independent experiments plotted as mean ± SEM. Statistical comparisons (ns, $P > 0.05$; *, $P \le 0.05$; **, $P \le 0.01$; ***, $P \le 0.001$; ****, $P \le 0.0001$; in comparison with the *psd1Δ* control) were performed by one-way ANOVA with Dunnett multiple comparisons test. **(D)** Yeast strains of the indicated genotype (at left) were dilution spotted onto solid glucose minimal medium either supplemented with Etn (2mM) or not as indicated at top. Results were recorded after 72 h of incubation at 30°C. Restoration of growth in the absence of Etn identifies partial reactivation of the Psd2 pathway in *psd1Δstt4^{pstB1}* mutants. **(E)** Isogenic yeast strains with the designated genotypes (at left) were spotted in 10-fold dilution series on solid synthetic complete medium with or without Etn (2 mM) and incubated at 30°C for 72 h.

model for functional dissection of a candidate MCS. The *PSD* system has been exploited to that end and, in the case of Psd2, a combination of genetic and protein interaction data have been incorporated into a current model proposing that endosomal Psd2-dependent PtdSer decarboxylation requires assembly of an ER-endosomal MCS (Fig. 1 A; Riekhof et al., 2014; Voelker, 2005).

Herein, we demonstrate that intrinsic Psd2 activity is independent of the known molecular tethers proposed as components of a Psd2 MCS. We further show that Psd2 interacts with both a phosphatidylinositol transfer protein (PITP) and a phosphatidylinositol (PtdIns) 4-OH kinase independently, and establish that the PITP::Psd2 interaction is directly required for biologically sufficient activation of Psd2. Surprisingly, the activation mechanism, while dependent on the ability of PITP to physically engage Psd2, is independent of PITP activity as a PtdIns-transfer protein. Our results also suggest that PtdIns 4-OH kinase involvement in regulating Psd2-mediated PtdSer decarboxylation is complex and is exerted by indirect mechanisms, although the data hold out the formal possibility of a direct involvement as well. The collective data establish that the ER-endosomal MCS model in its present form represents an unsatisfactory description of the yeast Psd2 system, demonstrating the need for physiologically relevant assays for mechanistic dissections of MCS function.

Results

VAP family proteins and Pbi1 are dispensable for Psd2 pathway activity

The *PSD* system has been exploited using various approaches to arrive at a model that posits that endosomal Psd2-dependent PtdSer decarboxylation requires assembly of a specialized ER-endosomal contact site composed of Psd2, the Sfh4/Pdr17 PITP, the Stt4 PtdIns 4-OH kinase, the ER-localized VAP family tethering factor Scs2, and a functionally uncharacterized protein Pbi1 (YPL272C; Fig. 1 A; Riekhof et al., 2014; Voelker, 2005). Multiple lines of evidence fail to identify any positive roles for Scs2 and Pbi1 in Psd2 pathway activity in cells. Individual deletion of the *PSD2* and *SFH4* structural genes inactivated PtdSer decarboxylation through the Psd2 pathway, as assessed by each deletion allele conferring Etn auxotrophy on a *psd1Δ* mutant deficient in the metabolically redundant mitochondrial pathway for PtdSer decarboxylation to PtdEtn (Fig. 1 B). However, in agreement with the findings of Riekhof et al. (2014), individual deletion of neither the *PBI1* nor the *SCS2* structural genes had any such effect (Fig. 1 B). Deletion of the *SCS22* gene, which encodes the second Scs2-like protein in yeast, similarly had no deleterious effect on growth of *psd1Δ* cells on Etn-free medium. Indeed, even combinatorial ablation of both the *SCS2* and *SCS22* structural genes failed to impair Psd2-dependent PtdSer decarboxylation in cells as judged by phenotypic criteria (Fig. 1 B).

We considered the possibility that flux through the Psd2 pathway in cells might operate in excess of biological threshold and that the observed Etn prototrophies failed to report significant, yet phenotypically silent, roles for Scs2 and Pbi1 in promoting metabolic flux through this pathway. That possibility was contraindicated by [^{3}H]-serine metabolic labeling experiments that monitored Psd2-dependent conversion of [^{3}H]-PtdSer to [^{3}H]-PtdEtn in vivo. Using the [^{3}H]-PtdEtn/[^{3}H]-PtdSer ratio as readout of Psd2 pathway activity, a significant decrease in the [^{3}H]-PtdEtn/[^{3}H]-PtdSer ratio was measured in the *psd1Δ sfh4Δ* double mutant relative to the *psd1Δ* positive control (Fig. 1 C). Individual ablation of either Pbi1, Scs2, or Scs22 activities, or combinatorial inactivation of both Scs2 and Scs22, failed to compromise the efficiency of Psd2-mediated PtdSer decarboxylation in cells.

To interrogate potentially antagonistic functional interactions, we tested whether inactivation of Pbi1, Scs2, and/or Scs22 rescued Psd2 pathway activity in *sfh4Δ* and/or *stt4^{pstB1}* mutants. The *stt4^{pstB1}* allele was identified in the original genetic screen for mutants presumed to be defective in Psd2 activity (Trotter et al., 1998). In no case did we observe phenotypic rescue upon incorporation of *pbi1Δ*, *scs2Δ*, or *scs22Δ* alleles into a *psd1Δ sfh4Δ* genetic background. The isogenic *pbi1Δ*, *scs2Δ*, and *scs22Δ* derivatives consistently maintained the Etn auxotrophy characteristic of the parental *psd1Δ sfh4Δ* strain (Fig. 1 D). Interestingly, *scs2Δ* (but not *pbi1Δ* or *scs22Δ*) and *scs2Δ scs22Δ* enabled visible growth of the *psd1Δstt4^{pstB1}* mutant on Etn-free medium. This phenotype was accompanied by a reproducible 1.4-fold increase in [^{3}H]-PtdEtn/[^{3}H]-PtdSer ratio for the *psd1Δ stt4^{pstB1} scs2Δ* mutant relative to the isogenic *psd1Δstt4^{pstB1}* control (Fig. S1 A). Thus, if anything, the VAP family protein Scs2 interferes with, rather than promotes, Stt4 involvement in Psd2-dependent PtdSer decarboxylation in cells.

Psd2 pathway activity is not modulated by individual *OSH* protein function

Previous studies established an antagonistic interaction between a specific member of the yeast oxysterol binding protein family (Kes1 or Osh4) and the major yeast PITP Sec14 in the regulation of PtdIns-4-phosphate (PtdIns4*P*) signaling (Fang et al., 1996; Huang et al., 2018; Li et al., 2002). Given the proposal that Osh proteins are functional components of intermembrane contact sites (Stefan et al., 2011; Tian et al., 2018), and given that Osh6 and Osh7 show PtdSer/PtdIns4*P* transfer activity in vitro (Chung et al., 2015b; Moser von Filseck et al., 2015), we considered the possibility that *OSH* proteins are involved in the Psd2 pathway. However, neither individual deletion of each *OSH* gene nor *OSH6* or *OSH7* overexpression was of any consequence to the growth of *psd1Δ* cells on Etn-free medium (Figs. 1 E and S1 B). In addition, neither deletion of any single *OSH* gene nor overexpression of *OSH6* or *OSH7* restored significant growth to either *sfh4Δpsd1Δ* or *psd1Δstt4^{pstB1}* cells on Etn-free medium (Figs. 1 E and S1, B and C). The phenotype of *osh6Δ osh7Δ* double mutants in a *psd1Δ* genetic background is described below.

Psd2 pathway activity was similarly indifferent to ablation of the structural genes encoding other tethers (i.e., the endosomal tether Vps13 and ER-Golgi tethers Lam5 or Lam6; De et al., 2017; Elbaz-Alon et al., 2015; Gatta et al., 2015; Kumar et al., 2018; Murley et al., 2015) when assessed phenotypically in *psd1Δ* genetic backgrounds (Fig. S1 D). Importantly, while all of these directed assays could have overlooked an important factor not previously suggested in the literature, a systematic survey of all nonessential yeast genes failed to identify any functions other

than Sfh4 and Psd2 that are required for growth of *psd1Δ* cells in Etn-free medium (Fig. S1 E and Table S1). These cumulative analyses support the idea that Sfh4 and Stt4 are the two primary components that individually exert significant control over Psd2-mediated PtdSer decarboxylation in cells.

Stt4 PtdIns 4-OH kinase activity is required for Etn prototrophy in cells expressing Psd2 as sole PtdSer decarboxylase

Cell-free lysates prepared from *stt4^{pstB1}* cells exhibit reduced PtdIns 4-OH kinase activity in vitro (Trotter et al., 1998). As those data are subject to multiple interpretations, several lines of experimentation were conducted to directly assess whether Stt4 enzymatic activity was required for the Etn prototrophy of cells expressing Psd2 as sole source of PtdSer decarboxylase activity. As first step, the *stt4^{pstB1}* allele was recovered from genomic DNA and the *STT4* nucleotide sequence determined in its entirety. *STT4* encodes a 1901-aa PtdIns 4-OH kinase, and the *stt4^{pstB1}* allele differed from the WT *STT4* nucleotide sequence by a single G→A transition mutation located within the Stt4 catalytic domain. This domain is bounded by residues 1641 and 1848 (http://pfam.xfam.org/protein/P37297), and the *pstB1* mutation substitutes Gly with Asp at aa 1782 (Fig. 2 A). We henceforth refer to the *stt4^{pstB1}* allele as *stt4^{G1782D}*.

Two assays were employed to interrogate whether Stt4^{G1782D} is intrinsically defective in PtdIns4*P* production in situ. First, GFP-2xPH^{Osh2} was used as a PtdIns4*P* biosensor in vital imaging assays (Roy and Levine, 2004). This biosensor registers an Stt4-dependent plasma membrane (PM) PtdIns4*P* pool as well as a punctate TGN/endosomal PtdIns4*P* pool generated by the Pik1 PtdIns 4-OH kinase (Nile et al., 2014). In agreement with previous analyses of WT cells (Nile et al., 2014), ∼91% of the *psd1Δ STT4* control cells displayed localization of the biosensor to both PM and punctate TGN/endosomal structures. A minor fraction of cells (∼9%) exhibited a solely PM localization profile (Fig. 2 B). By contrast, only 44% of *psd1Δ stt4^{G1782D}* cells showed PM staining with this reporter (along with punctate TGN/endosomal staining), and 56% of cells displayed solely punctate TGN/endosomal localization of the reporter with no visible PM staining at all (Fig. 2 B). Those imaging results reported compromise of Stt4-mediated PtdIns4*P* production in *stt4^{G1782D}* cells.

Supporting data were obtained from metabolic [^{3}H]-inositol radiolabeling experiments coupled to analyses of Stt4-dependent PtdIns4*P* production. These measurements exploited *sac1Δ* mutants deficient in the Sac1 PtdIns4*P* phosphatase, i.e., the dominant activity for degradation of Stt4-generated PtdIns4*P* in yeast (Foti et al., 2001; Guo et al., 1999; Nemoto et al., 2000; Rivas et al., 1999). As a result, these measurements directly reported Stt4 PtdIns 4-OH kinase activity in vivo. Indeed, *stt4^{G1782D}* mutants displayed significant reductions in PtdIns4*P* levels relative to isogenic *STT4* control cells (Fig. 2 C).

To confirm that PtdIns 4-OH kinase activity was required for Stt4 function in promoting Psd2-mediated PtdSer decarboxylation in cells, the consequences of expressing a catalytic dead version of Stt4 in *psd1Δ stt4^{G1782D}* yeast were determined. Design of the catalytic-dead *stt4^{D1754A}* allele was guided by characterization of the kinase-dead *pik1^{D918A}* allele (Strahl et al., 2005). Low-copy yeast centromeric (*CEN*) plasmids carrying *STT4*, *stt4^{G1782D}*, or *stt4^{D1754A}* expression cassettes driven by the natural *STT4* promoter were used in these analyses. Whereas individual expression of *STT4* or *stt4^{G1782D}* was sufficient to rescue viability of an *stt4^{ts}* mutant strain at a restrictive temperature of 37°C, *stt4^{D1754A}* expression failed to do so (Fig. S2 A). When these same expression constructs were introduced into the *psd1Δ stt4^{G1782D}* mutant, only *STT4* expression supported growth of *psd1Δ stt4^{G1782D}* cells on Etn-free medium (Fig. S2 B). Thus, both *stt4^{G1782D}* and *stt4^{D1754A}* scored as defective alleles. This defect was not a trivial result of enzyme instability, as both Stt4^{G1782D} and Stt4^{D1754A} are stable proteins in vivo (Fig. S2 C). These data indicated that (a) PtdIns 4-OH kinase activity of Stt4 was required for its involvement in the Psd2 pathway, (b) Stt4^{G1728D} represents a functional hypomorph with reduced in vivo lipid kinase activity, and (c) this crippled enzyme, while sufficiently functional to support yeast cell viability, was inadequate for restoration of Etn prototrophy to yeast expressing Psd2 as sole PtdSer decarboxylase activity.

The yeast Stt4 PtdIns 4-OH kinase catalytic domain requires accessory proteins for biologically sufficient activity, and it assembles into two distinct complexes in that regard. One consists of the Stt4 catalytic subunit with the associated Ypp1 and Erf3 subunits, whereas the other consists of Stt4 and the accessory subunits Erf3 and Sfk1 (Audhya and Emr, 2002; Baird et al., 2008; Baskin et al., 2016; Chung et al., 2015a; Nakatsu et al., 2012). Of these, Sfk1 is the only activity dispensable for cell viability. We found that *psd1Δ sfk1Δ* double mutant yeast were not compromised for growth on Etn-free medium (Fig. S2 D), indicating that Stt4 complex II was not required for Psd2 pathway activity in vivo. Overexpression of Ypp1, Efr3, or Sfk1 neither evoked Etn auxotrophy in *psd1Δ* yeast nor did enhanced expression of these noncatalytic subunits rescue the Etn auxotrophy of *psd1Δ stt4^{G1782D}* cells (Fig. S2 E).

The PtdIns-binding substructure of Sec14-like PITPs is conserved in Sfh4

Sec14 and its related PITPs potentiate PtdIns 4-OH kinase activities in cells (including Stt4) by a presentation mechanism that renders PtdIns a superior substrate for the lipid kinase (Bankaitis et al., 1989, 2010; Schaaf et al., 2008). The biological specificities that come with the presentation model are striking: of the six Sec14-like PITPs in yeast, Sfh4 is unique in its involvement with the Psd2 pathway (Fig. S3 A). Thus, we considered the possibility that Sfh4 acts in a canonical fashion by enhancing Stt4 activity to expand production of a PtdIns4*P* pool dedicated to activation of the Psd2 pathway. This hypothesis predicted that Sfh4 mutants unable to bind PtdIns would be defective in the context of Psd2-mediated PtdSer decarboxylation. To identify Sfh4 residues critical for PtdIns-binding, the Sfh4 primary sequence was threaded onto a high-resolution crystal structure of Sfh3 bound to PtdIns. Sfh3 is the most similar of the yeast PITPs to Sfh4 (49% primary sequence identity; 65% similarity). The optimized Sfh4::PtdIns homology model described a Sec14-fold comprising 11 α-helices, six 3_{10}-helices, and five β-strands (Fig. S3 B; Schaaf et al., 2008; Sha et al., 1998). The common PtdIns-coordination substructure

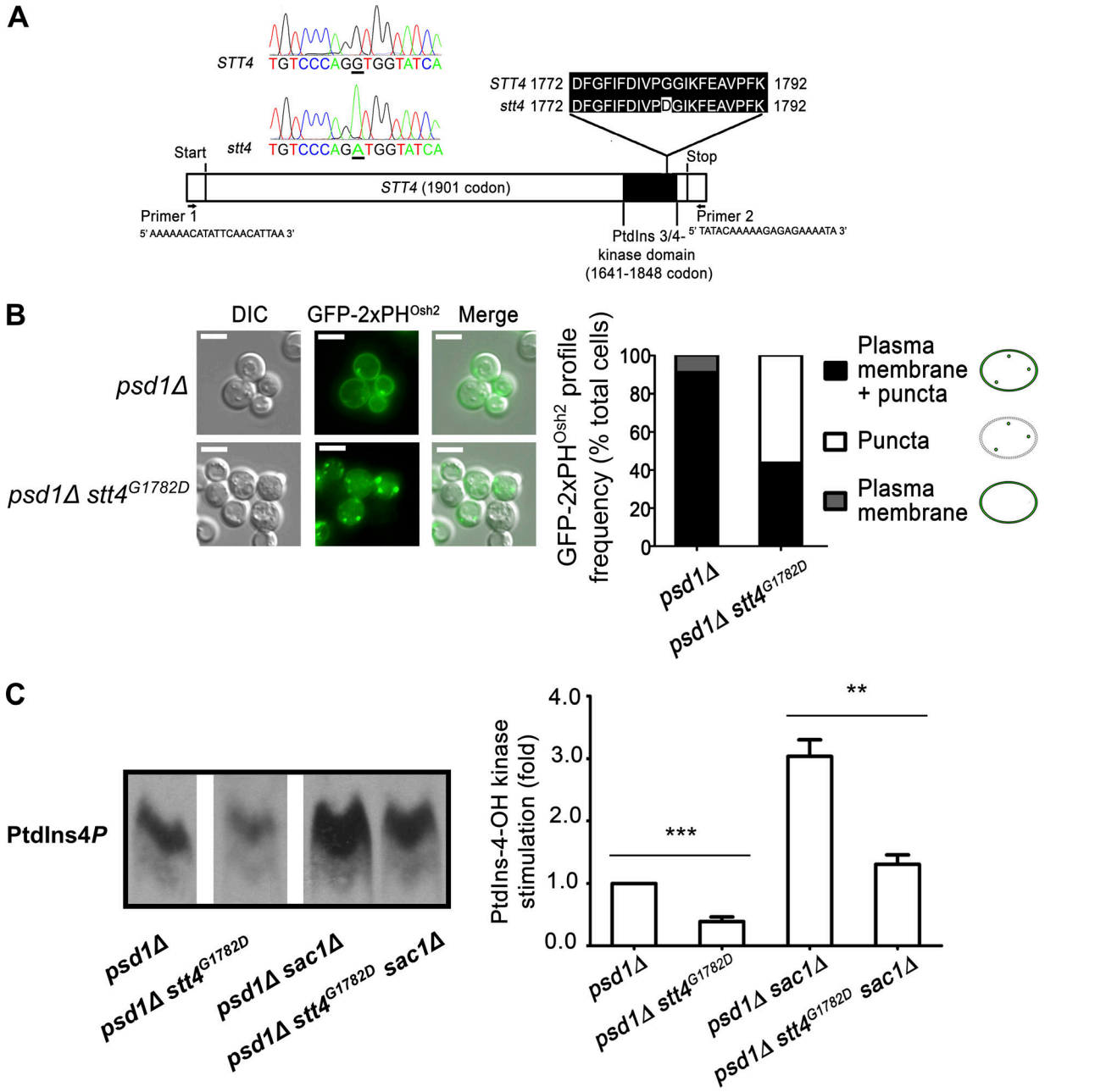

Figure 2. **Stt4 PtdIns 4-OH kinase activity is required for biologically sufficient Psd2 activity. (A)** The full-length *STT4* gene was recovered from the *pstB1* mutant genome, and DNA sequence analysis identified a $G_{1782}D$ missense substitution in the PtdIns-kinase domain. **(B)** Distributions of the GFP-2xPH^{Osh2} PtdIns4*P* biosensor in *psd1Δ* and *psd1Δ stt4^{G1782D}* cells were determined by fluorescence microscopy imaging and classified for each cell imaged as PM localization, punctate TGN/endosomal localization, or both (left panel; bar = 5 µm). The fractional representation of cells exhibiting each distribution profile is shown (right panel; $n > 300$). The PM localization of the biosensor reads out the Stt4-dependent PtdIns4*P* pool. **(C)** Appropriate yeast strains (genotypes at bottom) were radiolabeled to steady-state with [^{3}H]-inositol. The *sac1Δ* strains were used to enhance the PtdIns4*P* signal and emphasize the PtdIns4*P* synthesis contribution to the data. Phospholipids were extracted and resolved by TLC and autoradiography (left panel; the retention factor of the PtdIns4*P* band is 0.5322). All images were collected from the same TLC plate. PtdIns4*P* band intensities were measured by densitometry (arbitrary units) and expressed as a ratio of PtdIns4*P* to total input cpm (input range from 1,070,088 to 1,627,675 cpm). The normalized ratios were related to a *psd1Δ* control (set to 1.0; right panel). Values represent averages from three independent experiments plotted as mean ± SEM. Statistical comparisons of values used the unpaired two-tailed *t* test. ***, $P \le 0.001$ in comparison to the *psd1Δ* strain; **, $P \le 0.01$ in comparison to the *psd1Δ sac1Δ* strain.

essential for specific PtdIns binding observed in crystal structures of other Sec14-like proteins was clearly recognized in the Sfh4 structural model (Fig. S3 C; Phillips et al., 1999; Ren et al., 2014; Schaaf et al., 2008). Of note in that regard are Sec14 residues T_{236} and K_{239}, which play critical roles in PtdIns headgroup binding and are conserved throughout the Sec14 superfamily (Schaaf et al., 2008). The Sfh4 cognates of those residues are Sfh4^{T266} and Sfh4^{K269} (Fig. S3 D). Thus, Sfh4^{T266D,K269A} and Sfh4^{T266W,K269A} double mutants were expected to be defective for PtdIns binding based on electrostatic and steric considerations.

Biochemical validation of Sfh4 mutants defective in PtdIns binding

Consistent with expectations, both Sfh4^{T266D,K269A} and Sfh4^{T266W,K269A} exhibited strong PtdIns-binding deficits as determined by three lines of evidence. First, recombinant Sfh4, Sfh4^{T266D,K269A}, and Sfh4^{T266W,K269A} proteins were purified from *Escherichia coli* and queried for PtdIns-transfer activity in vitro using an assay that quantifies mobilization of [^{3}H]-PtdIns from donor rat liver microsomes to acceptor PtdCho vesicles. Whereas both Sfh4 and Sec14 catalyzed robust PtdIns-transfer, neither Sfh4^{T266D,K269A} nor Sfh4^{T266W,K269A} exhibited significant activity (Figs. 3 A and S3 E). Second, as independent confirmation of the [^{3}H]-PtdIns transfer assay, the activities of Sfh4 and mutant proteins were assayed in a real-time fluorescence dequenching PtdIns-transfer system (Somerharju et al., 1987). In this assay, transfer is scored by increased fluorescence of pyrene-labeled PtdIns ([Pyr]-PtdIns) upon its mobilization from the quenching environment provided by the donor vesicles. Again, Sfh4 catalyzed robust transfer of [Pyr]-PtdIns, whereas Sfh4^{T266D,K269A} was strongly deficient (Fig. S3 F). Third, whereas enhanced *SFH4* expression rescued growth of a *sec14-1^{ts}* mutant at the restrictive temperature of 37°C, elevated expression of neither Sfh4^{T266D,K269A} nor of Sfh4^{T266W,K269A} elicited detectable phenotypic rescue of the *sec14-1^{ts}* growth defect (Fig. 3 B). This failure was not the trivial consequence of mutant Sfh4 protein instability, as immunoblotting experiments demonstrated that both mutant proteins accumulated in cells to levels comparable to those of Sfh4 itself (Fig. 3 C).

Finally, [^{3}H]-inositol radiolabeling experiments confirmed that both Sfh4^{T266D,K269A} and Sfh4^{T266W,K269A} were defective in stimulating Stt4-mediated PtdIns4*P* production in vivo. Those measurements were conducted in a *sac1Δ sec14-1^{ts}* double mutant background using a previously established experimental design (Ile et al., 2010; Schaaf et al., 2008). Briefly, the *sac1Δ* allele inactivates the primary pathway for degradation of the PtdIns4*P* produced by Stt4. The *sec14-1^{ts}* allele erases the dominant stimulatory effect of Sec14 on Stt4 in vivo activity when cells are incubated at 37°C, thereby providing an assay for assessing the stimulatory effects of enhanced expression of Sfh4 and mutants of interest on Stt4 activity. Whereas *SFH4* expression supported a ∼2.5-fold stimulation of PtdIns4*P* synthesis relative to vector control, cells expressing Sfh4^{T266D,K269A} or Sfh4^{T266W,K269A} exhibited only basal PtdIns4*P* levels that were comparable to those of the negative control (Fig. 3 D). Thus, while Sfh4 effectively stimulated Stt4 activity in vivo, neither Sfh4^{T266D,K269A} nor Sfh4^{T266W,K269A} was able to do so.

Sfh4 mutants defective in PtdIns binding maintain competence in promoting Psd2 pathway activity in vivo

Contrary to expectations that Sfh4 must bind PtdIns to function in the Psd2 pathway, expression of either Sfh4^{T266D,K269A} or Sfh4^{T266W,K269A} was sufficient to restore Etn prototrophy to a *psd1Δ sfh4Δ* double mutant yeast strain. This level of rescue was phenotypically indistinguishable from that observed for the Sfh4 control, even when the mutant proteins were expressed from cassettes driven by the weak *SFH4* promoter (Fig. 3 E). This result deserves emphasis, as the expression cassettes were all carried on low-copy centromeric vectors: that is, a configuration that supported a physiologically appropriate level of Sfh4 expression. Further testimony to the functionality of these PtdIns-binding defective Sfh4 mutants was provided by [^{3}H]-serine labeling experiments. The efficiencies of Psd2-dependent conversion of [^{3}H]-PtdSer to [^{3}H]-PtdEtn were comparable, irrespective of whether Sfh4, Sfh4^{T266D,K269A} or Sfh4^{T266W,K269A} represented the sole sources of Sfh4 activity in the cell (Fig. 3 F).

That activation of the Psd2 pathway was not a simple result of Sfh4-stimulated PtdIns4*P* production by the Stt4 PtdIns 4-OH kinase was supported by two other lines of evidence. First, inactivation of the Sac1 PtdIns4*P* phosphatase was insufficient to produce either a bypass Sfh4 condition for Psd2-dependent decarboxylation of PtdSer in *psd1Δ sfh4Δ* mutants or to rescue Psd2 pathway activity in *psd1Δ stt4^{GI782D}* mutants (Fig. S3 G). Genetic ablation of Sac1 PtdIns4*P* phosphatase activity elevates the levels of PtdIns4*P* generated by Stt4 some 10-fold (Audhya and Emr, 2002; Cleves et al., 1989; Foti et al., 2001; Guo et al., 1999; Nemoto et al., 2000; Rivas et al., 1999). Those negative results were also recapitulated in genetic backgrounds in which each of the other yeast synaptojanin-like phosphoinositide phosphatase structural genes were individually deleted (Stefan et al., 2002; Fig. S3 H).

Isolation of Sfh4 mutants specifically defective in stimulating Psd2 activity

To determine what Sfh4 properties are required for its positive involvement in Psd2-dependent PtdSer decarboxylation, we sought Sfh4 mutants with defects restricted to the Psd2 activation function. To that end, an unbiased genetic screen was designed to identify Sfh4 mutants specifically defective in Psd2 activation. This screen coupled mutagenic PCR with gap repair of a centromeric *SFH4* expression plasmid in a *ura3 sfh4Δ psd1Δ sec14^{ts}* recipient strain (Fig. S4 A). Expression of a mutant Sfh4 incompetent for activation of the Psd2 pathway would fail to impart Etn prototrophy to the strain. The recipient strain had the additional feature that it could not grow at 37°C because it carries a *sec14-1^{ts}* allele. This feature was exploited to filter away trivial *sfh4* loss-of-function mutations, as the repaired plasmid drives expression of the mutagenized *SFH4* ORF from the powerful constitutive *PGK* promoter, a configuration sufficient to support growth of the *sec14-1^{ts}* recipient at 37°C if the expressed Sfh4 protein is a functional PITP. Thus, gap-repaired Ura$^+$ transformants of the *ura3 sfh4Δ psd1Δ sec14^{ts}* recipient strain were selected and screened by replica plating for colonies displaying the dual unselected traits of (a) Etn auxotrophy (mutant Sfh4 fails to activate the Psd2 pathway) and (b) the ability to form colonies at 37°C (mutant Sfh4 retains sufficient PITP activity to act as functional surrogate for Sec14).

From a total of >8,000 Ura$^+$ transformants so analyzed, a single isolate was identified that exhibited the desired unselected phenotypes of Etn auxotrophy and ability to grow at 37°C. The plasmid was recovered from the yeast isolate and retransformed into a naive *ura3 sfh4Δ psd1Δ sec14^{ts}* recipient strain using Ura$^+$ selection. The Ura$^+$ transformants again displayed the unselected Etn auxotrophy and thermoresistant growth traits, thereby confirming plasmid linkage of these hallmark

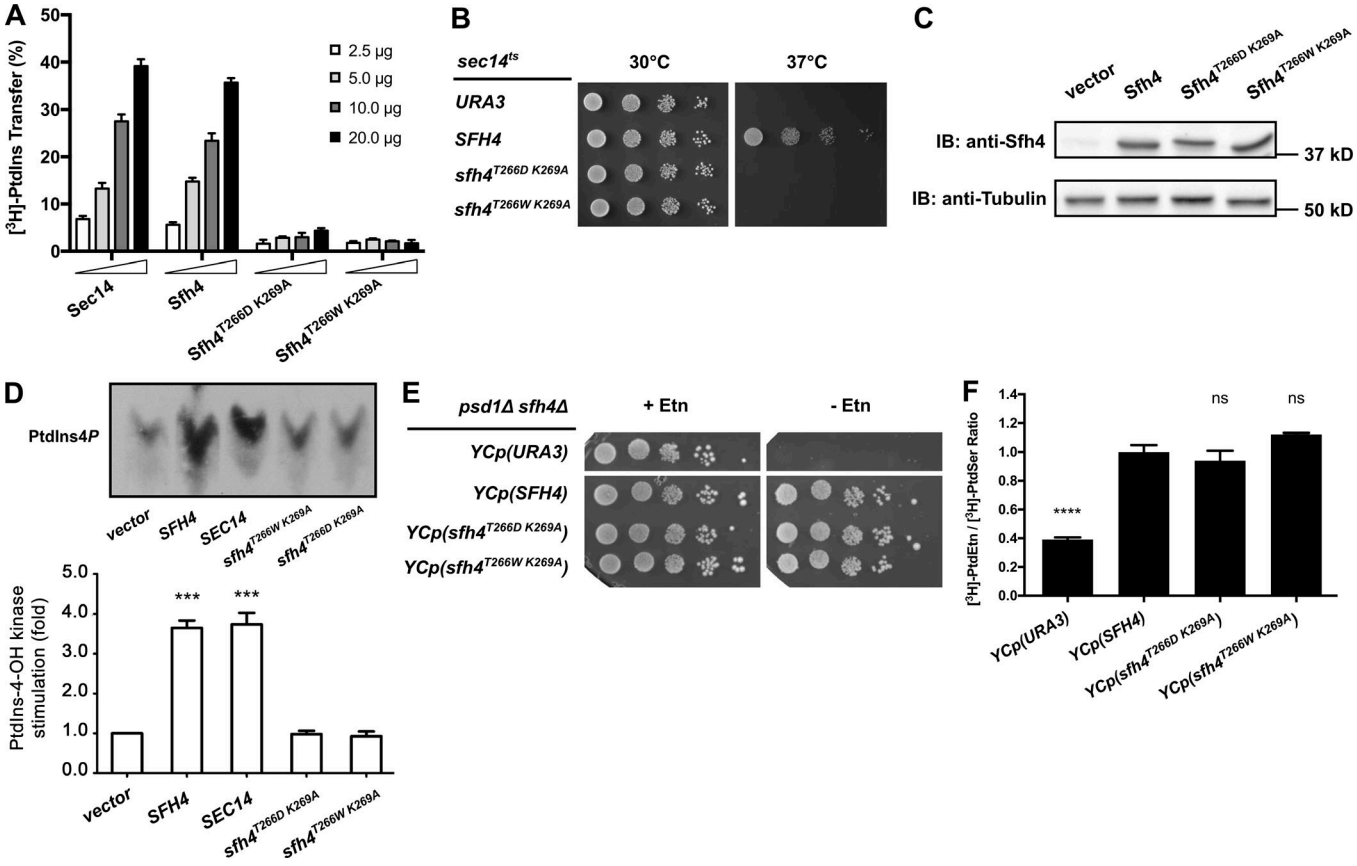

Figure 3. **Sfh4 mutants defective for PtdIns binding retain ability to potentiate Psd2 activity in vivo. (A)** PtdIns transfer assays for WT and mutant Sfh4 proteins. The indicated step series of purified recombinant Sec14, Sfh4, Sfh4$^{T266D\ K269A}$, and Sfh4$^{T266W\ K269A}$ were assayed for PtdIns transfer from rat liver microsomes to acceptor vesicles. Transfer activity is expressed as the ratio of [^{3}H]-PtdIns in the acceptor vesicle fraction to total input [^{3}H]-PtdIns in donor vesicle fraction × 100%. Values represent averages from three independent experiments plotted as mean ± SEM. [^{3}H]-PtdIns inputs ranged in these assays from 5,559 to 5,935 cpm, with background transfer ranging from 546 to 670 cpm (determined in mock samples where buffer was incorporated rather than protein). **(B)** Isogenic *sec14^{ts}* yeast transformed with a mock *YCp(URA3)* vector or *YCp(URA3)* vectors carrying *SFH4* WT, *sfh4$^{T266D\ K269A}$* or *sfh4$^{T269W\ K269A}$* expression cassettes under *PGK1* promoter control were spotted in 10-fold dilution series on uracil-free medium and incubated at the permissive and restrictive temperatures of 30°C and 37°C, respectively. Growth at 37°C signifies that the protein of interest is competent for PtdIns binding/exchange. **(C)** Immunoblots of lysates prepared from *psd1Δ sfh4Δ* yeast carrying the designated YCp vector where expression of the proteins of interest was driven by the strong constitutive *PGK1* promoter. Equal amounts of total protein were loaded. Sfh4 and tubulin (normalization control) were visualized with anti-Sfh4 or anti-tubulin antibodies, respectively. **(D)** Left: Isogenic *sec14^{ts} sac1 sfh4Δ* yeast mutants ectopically expressing the indicated Sec14 or Sfh4 proteins from a yeast centromeric vector where the expression cassette was driven by the *PGK1* promoter were radiolabeled to steady state with [^{3}H]-inositol and shifted to 37°C for 3 h. Phospholipids were extracted, and PtdIns4*P* was resolved by TLC (Phillips et al., 1999; Schaaf et al., 2008; see Materials and methods; the retention factor value of the PtdIns4*P* band is 0.4943). The vector and *SEC14* derivatives represented negative and positive controls, respectively. Right: PtdIns4*P* band intensities were measured by densitometry and expressed as a ratio of PtdIns4*P*/total input counts (inputs ranged from 1,332,937 to 1,804,138 cpm). These normalized ratios were related to a vector control (set to 1.0 on the relative scale). Values represent averages from three independent experiments plotted as mean ± SEM. Statistical comparisons of values used the unpaired two-tailed *t* test. ***, P ≤ 0.001 in comparison with a vector control. **(E)** Isogenic *psd1Δ sfh4Δ* yeast transformed with the mock *YCp(URA3)* vector, or with *YCp(URA3)* vectors expressing the indicated genes from the natural *SFH4* promoter, were spotted in 10-fold dilution series on uracil-free medium with or without supplementation with 2 mM Etn as indicated at top. Plates were incubated at 30°C for 72 h. **(F)** Psd2-mediated PtdSer decarboxylation is supported by Sfh4 mutants defective in PtdIns binding/exchange. The yeast strains described for E were incubated with [^{3}H]-Ser for 3 h at 30°C, phospholipids were extracted, and PtdSer and PtdEtn were resolved by TLC. Decarboxylation of PtdSer to PtdEtn was expressed as a [^{3}H]-PtdEtn/[^{3}H]-PtdSer ratio for the indicated strains and related to the [^{3}H]-PtdEtn/[^{3}H]-PtdSer ratio of the *SFH4* control strain (set as 1.0). Values represent the mean ± SEM from at least three independent experiments. Statistical comparisons (ns, P > 0.05; ****; P ≤ 0.0001) were to the *SFH4* control and were performed by one-way ANOVA with the Dunnett multiple comparisons test.

phenotypes. Nucleotide sequence analyses of the plasmid-borne *SFH4* identified a single TTT→CTT transition mutation in *SFH4* codon 175 that substituted Phe at that position with Leu. Mapping of this substitution onto the threaded Sfh4 structural model projected that residue F_{175} lies on the surface of the open conformer of this PITP at a position far removed from the substructure that coordinates PtdIns headgroup binding (Fig. 4 A).

Characterization of F_{175} substitutions reveals a gradient of functional defects

To probe the involvement of F_{175} in Sfh4 engagement with the Psd2 pathway, this residue was altered to a series of other amino acids of differing size, hydrophobicity, and charge. The abilities of the corresponding Sfh4 mutant proteins to activate the Psd2 pathway were then assessed. Expression of the mutant proteins

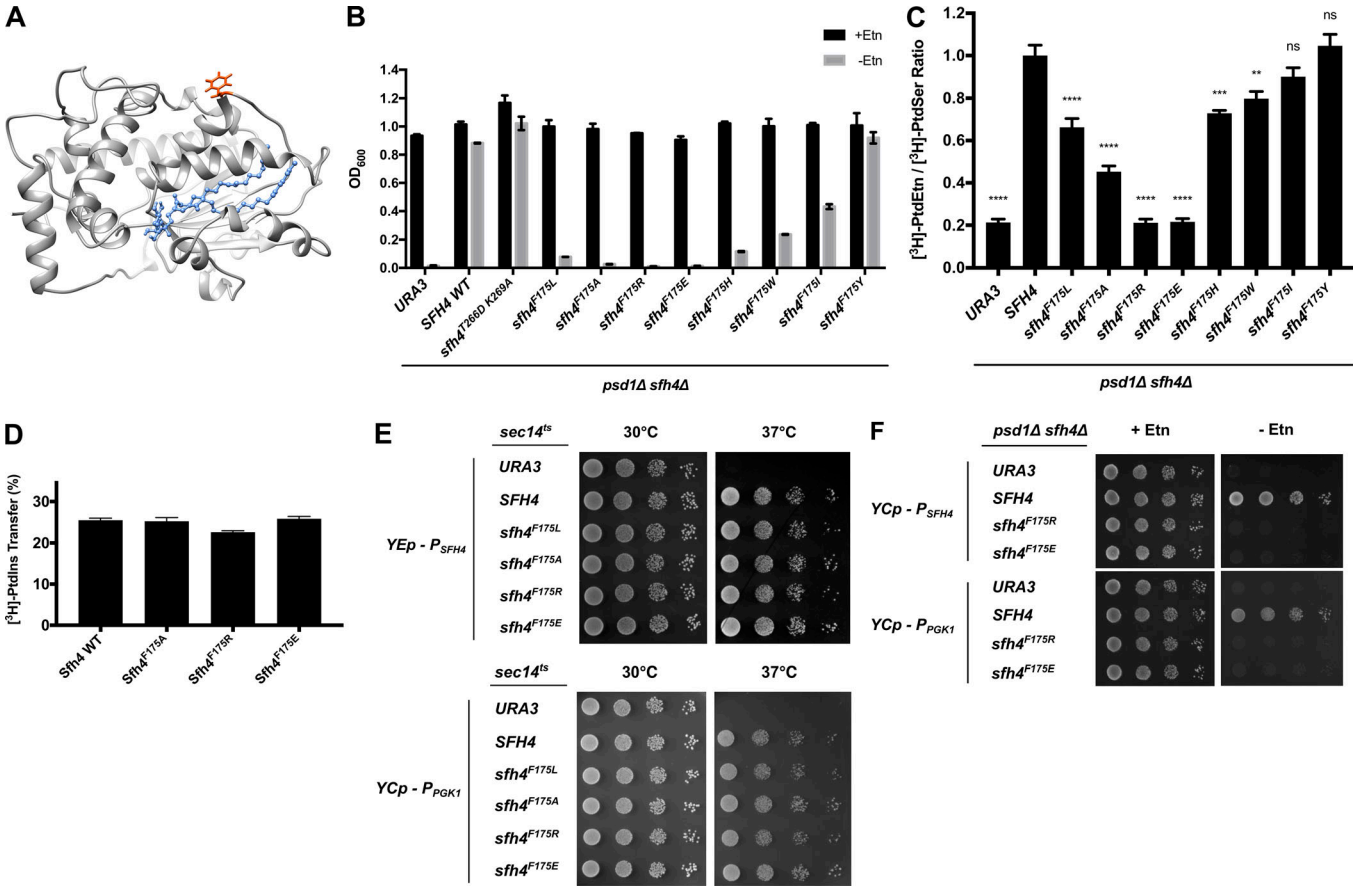

Figure 4. **Sfh4 mutants specifically defective in Psd2 pathway stimulation. (A)** Sfh4 homology model based on threading onto the Sfh3 crystal structure is shown, and residue F_{175} is highlighted in orange-red. The bound PtdIns molecule is rendered in blue ball and stick mode. **(B)** Growth phenotypes in Etn (2 mM)-containing (black bars) or Etn-free (gray bars) minimal medium lacking uracil of a parental *psd1Δ sfh4Δ* strain transformed with mock *YCp(URA3)* vector, or with *YCp(URA3)* vectors for expression of *SFH4* or individual *sfh4*^{F175} missense alleles (indicated at bottom). Cultures were initially grown in uracil-free Etn-replete minimal synthetic defined (SD) medium at 30°C to midlogarithmic phase. Cells were washed twice with water and resuspended in uracil-free Etn-replete minimal SD medium. After a 4-h incubation at 30°C to deplete any residual Etn stores, the cultures were washed one more time with water and diluted to an A_{600} of 0.01 in the appropriate minimal SD medium. The diluted cultures were incubated at 30°C for 46.5 h, and the A_{600} of each culture was recorded. Values represent averages from two independent experiments (n = 2) plotted as mean ± range. **(C)** PtdSer flux through the Psd2 pathway was measured as described in the legend to Fig. 1 C. Ectopic expression of the Sfh4 control and the test Sfh4^{F175} variants in the *psd1Δ sfh4Δ* parental strain was in all cases driven by an *SFH4* promoter cassette carried on a low-copy *CEN* plasmid. Decarboxylation of PtdSer to PtdEtn was expressed as a [^{3}H]-PtdEtn/[^{3}H]-PtdSer ratio for the indicated strains and related to the [^{3}H]-PtdEtn/[^{3}H]-PtdSer ratio of the *SFH4* control strain (set as 1.0). Values represent averages from at least three independent experiments plotted as mean ± SEM. Statistical comparisons to the *SFH4* control strain (ns, P > 0.05; **, P ≤ 0.01; ***, P ≤ 0.001; ****, P ≤ 0.0001) were performed using one-way ANOVA with the Dunnett multiple comparisons test. **(D)** Purified recombinant Sfh4, Sfh4^{F175A}, Sfh4^{F175R}, and Sfh4^{F175E} proteins (10 µg) were assayed for [^{3}H]-PtdIns-transfer activity as described in Materials and methods. Transfer activities are expressed as ratios of [^{3}H]-PtdIns in acceptor vesicle fractions relative to total input [^{3}H]-PtdIns present in donor vesicle fractions × 100%. Values represent averages from three independent experiments plotted as mean ± SEM. [^{3}H]-PtdIns inputs in these assays ranged from 11,317 to 11,724 cpm, while backgrounds ranged from 342 to 394 cpm. **(E)** Isogenic *sec14*^{ts} yeast transformed with an empty YEp vector or YEp vectors driving *SFH4* WT or *sfh4* mutant gene expression under *SFH4* promoter control (top panels), and isogenic *sec14*^{ts} yeast transformed with empty YCp vector or YCp vectors driving ectopic expression of *SFH4* or *sfh4* mutant gene expression from the *PGK1* promoter (bottom panels) were spotted in 10-fold dilution series on uracil-free medium and incubated at the permissive and restrictive temperatures of 30°C and 37°C, respectively. Growth at 37°C signifies ability of the corresponding protein to bind/exchange PtdIns and stimulate PtdIns 4-OH kinase activity in vivo. **(F)** Parental *psd1Δ sfh4Δ* yeast were transformed with a YCp(*URA3*) vector or derivatives harboring expression cassettes where transcription of *SFH4* or mutant *sfh4* genes was driven from either the *SFH4* promoter (P_{SFH4}) or the powerful *PGK1* promoter (P_{PGK1}). Transformants were spotted in 10-fold dilution series on uracil-free medium with or without exogenous Etn (2 mM) as indicated at top. Plates were incubated at 30°C for 72 h.

of interest was driven by the natural *SFH4* promoter, and the expression cassettes were introduced into the *psd1Δ sfh4Δ* parent strain on a centromeric low-copy (CEN) vector to approximate physiological levels of protein expression. The readout for Etn prototrophy was conducted in liquid medium, as this assay is a stricter gauge of Psd2 pathway activity than is the plate assay.

Sfh4^{F175Y} supported growth of the *psd1Δsfh4Δ* strain in Etn-free medium as efficiently as did expression of Sfh4 or expression of the PtdIns-binding-defective Sfh4^{T266D,K269A} mutants (Fig. 4 B). Sfh4^{F175W} and Sfh4^{F175H} were compromised in their ability to support cell growth in the absence of Etn, but this defect was not as severe as that recorded for Sfh4^{F175L}. The growth phenotypes were buttressed by [^{3}H]-serine metabolic

radiolabeling assays in which the [^{3}H]-PtdEtn/[^{3}H]-PtdSer ratio for Sfh4^{F175Y}-expressing cells was essentially the same as that of Sfh4-expressing cells. By contrast, the [^{3}H]-PtdEtn/[^{3}H]-PtdSer ratios of Sfh4^{F175W} and Sfh4^{F175H} cells were lower than those of Sfh4-expressing cells, but higher than those of cells reconstituted with Sfh4^{F175L} (Fig. 4 C). Sfh4^{F175A}–expressing cells were even more defective in stimulating Psd2 activity than were cells in which Sfh4^{F175L} was the sole source of Sfh4 function (Fig. 4, B and C). The most extreme defects were scored in cells relying on Sfh4^{F175R} and Sfh4^{F175E} for stimulation of Psd2 activity. Both proteins scored as completely defective in vivo (Fig. 4, B and C). All of these Sfh4^{F175} mutant proteins are stably expressed in vivo (Fig. S4 B).

For all Sfh4^{F175} mutants, the functional deficiencies in stimulating Psd2 pathway activity in vivo were on display even though Sfh4^{F175A}, Sfh4^{F175R}, and Sfh4^{F175E} exhibited WT [^{3}H]-PtdIns transfer activities in vitro (Figs. 4 D and S4 C). All of these mutant proteins similarly displayed WT rates of [Pyr]-PtdIns transfer in real-time fluorescence dequenching assays (Fig. S4 D). Moreover, Sfh4^{F175R} and Sfh4^{F175E} expression driven by either the weak *SFH4* promoter from a high-copy episomal plasmid-borne cassette, or driven by the powerful *PGK1* promoter from a low-copy *CEN* plasmid, was sufficient to rescue growth of *sec14^{ts}* yeast at the restrictive temperature of 37°C (Fig. 4 E). Yet, ectopic Sfh4^{F175R} and Sfh4^{F175E} expression from low-copy *CEN* plasmids, where transcription was driven by either the weak *SFH4* promoter or the powerful *PGK1* promoter, failed to restore growth of those cells in Etn-free medium. These data confirmed that both mutant proteins were specifically and dramatically defective for Psd2 pathway activation (Fig. 4 F).

Sfh4^{F175} substitutions compromise productive physical interaction with Psd2 in vivo

Previous studies claim Sfh4 binds Psd2, although no study addressed the physiological relevance of such an interaction (Gulshan et al., 2010; Riekhof et al., 2014). The availability of mutant Sfh4 proteins that show undiminished PITP activity, yet are strongly defective in stimulation of Psd2 pathway activity in vivo, afforded a system with which to directly interrogate whether Sfh4 and Psd2 engaged in a functionally relevant interaction. To this end, a coprecipitation assay was developed in which a C-terminal HA-tagged Psd2 was expressed from a multicopy plasmid in a yeast strain carrying a tandem affinity purification (TAP)-tagged *SFH4* allele transplaced into its natural genomic locus.

Indeed, Sfh4 and Psd2 exhibited an interaction as scored by efficient recovery of the tagged C-terminal 17-kD Psd2 α-subunit in an Sfh4-TAP coprecipitation regimen (Fig. 5 A). We conclude that this interaction occurred in situ and was not the trivial artifact of some postlysis association, as the coprecipitation was not reproduced when cells expressing only Sfh4-TAP were mixed with equal numbers of cells expressing only C-terminally HA-tagged Psd2 and the mixed suspension was lysed in the same vessel. Moreover, this interaction was judged to be specific, as no Psd2 was detected in control coprecipitations that offered a TAP-tagged version of the closely related Sfh3 PITP as bait (Fig. 5 A).

To determine whether Sfh4^{F175} mutants were compromised for the Psd2 interaction, the coprecipitation assay was repeated with TAP-tagged Sfh4^{F175L}, Sfh4^{F175A}, and Sfh4^{F175E} mutants. Those representative mutants span a range of deficiencies in Psd2 activity in vivo (in terms of magnitude of severity; Sfh4^{F175E} > Sfh4^{F175A} > Sfh4^{F175L}). The corresponding missense substitutions were incorporated into the genomic *SFH4-TAP* allele, the mutant Sfh4^{F175}-TAP proteins were recovered by affinity purification from cell-free lysates, and the coprecipitation fractions were interrogated for the HA-tagged Psd2 α-subunit. Satisfyingly, affinity purification of Sfh4^{F175L}-TAP demonstrated strongly reduced capture of the Psd2 α-subunit, whereas Sfh4^{F175A}-TAP was even more defective in this assay, and Sfh4^{F175E}-TAP failed to capture any Psd2 α-subunit at all (Fig. 5, B and D). Thus, the severities of Psd2-interaction defects for the Sfh4^{F175} mutants proportionately recapitulated the severities of the defects in Psd2-pathway activity in cells expressing these Sfh4^{F175} mutants as sole sources of Sfh4. Importantly, immunoblotting experiments demonstrated that, in all cases, the input cell-free lysate fractions contained similar levels of the HA-tagged Psd2 α-subunit. Those results indicated that neither Psd2 expression/stability nor the auto-processing activity of this enzyme was compromised in cells expressing Sfh4^{F175} mutants as their sole sources of Sfh4 activity.

Stt4 deficiencies do not compromise Sfh4-Psd2 interactions

To determine whether the in vivo Psd2::Sfh4 interaction was Stt4 dependent, we tested whether complex formation was compromised in the *stt4^{G1782D}* genetic background. To that end, the *stt4^{G1782D}* allele was transplaced into the *SFH4-TAP* yeast strain, clarified lysates were generated, and the coprecipitation assay repeated. As shown in Fig. 5, C and D, neither the Psd2-Sfh4 nor the crippled Psd2::Sfh4^{F175L} interactions were compromised in *stt4^{G1782D}* cells, even though the Stt4 deficiencies were of sufficient magnitude to render activity of the Psd2 pathway biologically insufficient for PtdEtn production. The fact that Stt4 deficiencies did not further diminish the already inefficient Psd2::Sfh4^{F175L} interaction argued that Stt4 catalytic activity has no role in chaperoning Psd2-Sfh4 complex formation.

Probing Stt4 interactions with Psd2

Analogous coprecipitation strategies using Stt4-TAP as bait were conducted to assess potential Stt4–Psd2 interactions (Fig. 6 A). Both Stt4-TAP and Stt4^{G1782D}-TAP were able to capture Psd2-HA, and this interaction met criteria for specificity on the basis of three controls: (a) comparable coprecipitation was not evident in colysis experiments controlling for postlysis association of Stt4-TAP and Psd2-HA, (b) no Psd2-HA was recovered in coprecipitations using a TAP-tagged Pik1 PtdIns 4-OH kinase as bait (thereby reproducing the in vivo specificity where the Stt4 PtdIns 4-OH kinase functions in Psd2 pathway activation whereas the Pik1 PtdIns 4-OH kinase does not; Fig. S5 A), and (c) Psd2-HA was not captured by Sfh3-TAP (Fig. 5 A). An important caveat regarding these coprecipitation experiments is that trace levels of postlysis Stt4-TAP::Psd2-HA association were consistently detected in colysis controls. But, as the levels of Psd2

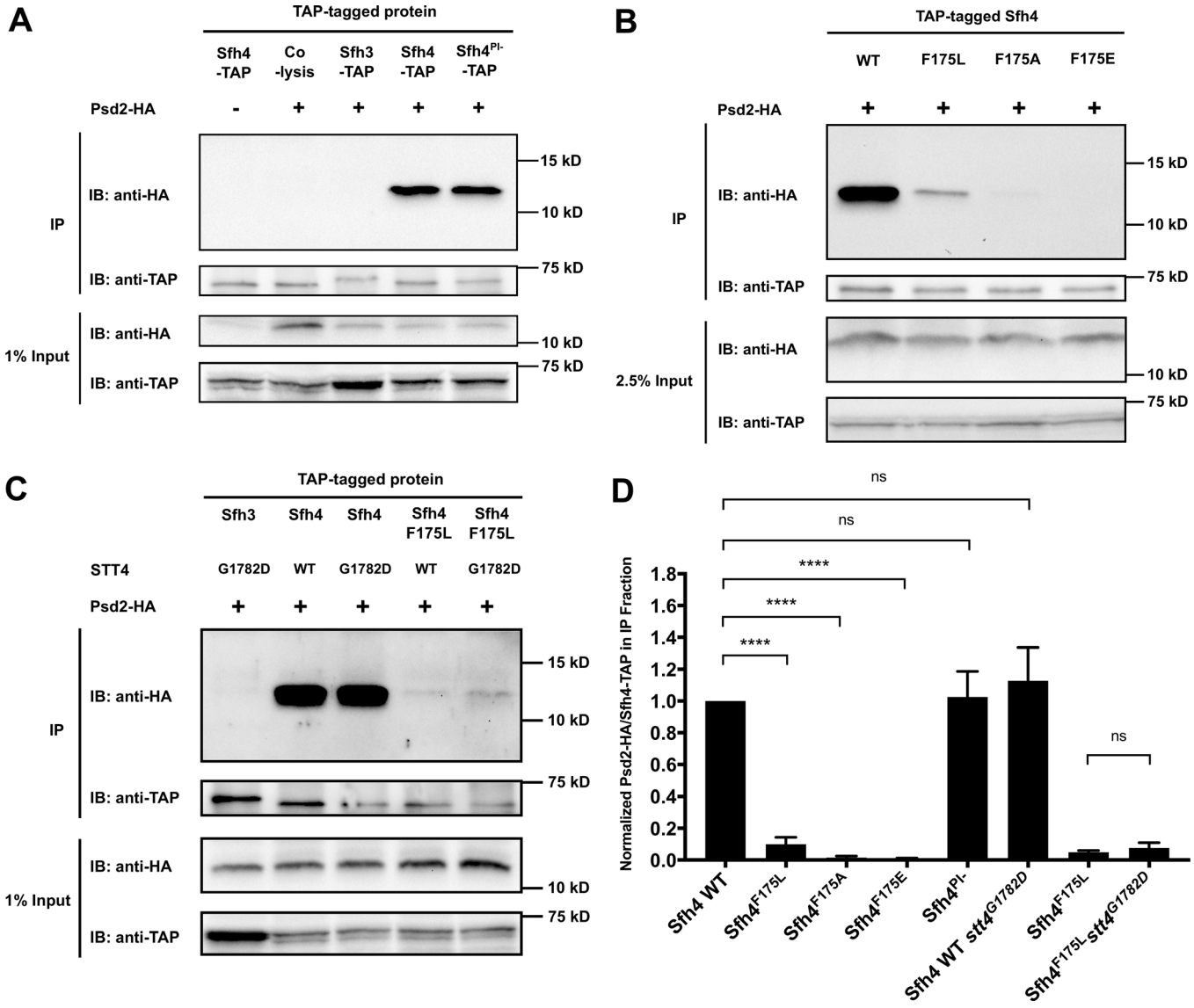

Figure 5. **Sfh4 interacts with Psd2 in vivo. (A)** WT yeast cells with integrated *SFH3-TAP*, *SFH4-TAP*, or *sfh4^{PI-}-TAP* (*sfh4^{T266D,K269A}-TAP*) cassette at their endogenous genome loci were transformed with yeast episomal plasmids driving Psd2-HA expression from the *PSD2* promoter (+) or with a mock episomal vector (–). Transformants were cultured to midlogarithmic growth phase, collected, and mechanically disrupted and clarified lysates were produced. Cell lysate aliquots (12 mg total protein) were subjected to anti-TAP immunoprecipitation (IP). All immunoprecipitated samples and input samples were processed for SDS-PAGE and immunoblotting (IB) with anti-HA or anti-TAP antibodies. In the colysis sample, WT yeast harboring YEp(*PSD2-HA*) and *SFH4-TAP*-expressing yeast were grown separately, and equal amounts (as measured by A_{600}) of each culture were mixed together and lysed in the same tube. The immunoprecipitation procedure was performed as described above. **(B)** WT yeast cells with integrated *SFH4-TAP*, *sfh4^{F175L}-TAP*, *sfh4^{F175A}-TAP*, and *sfh4^{F175E}-TAP* cassettes at their endogenous genomic loci were tested for their abilities to coprecipitate Psd2-HA expressed from a YEp vector as described in A. **(C)** Yeast cells carrying either a WT *STT4* allele or the mutant *stt4^{G1782D}* allele, and with integrated *SFH4-TAP* or *sfh4^{F175L}-TAP* cassettes at their endogenous genomic *SFH4* loci, were tested for their abilities to coprecipitate Psd2-HA expressed from a YEp vector as described in A. The *stt4^{G1782D}* was transplaced into the endogenous *STT4* genomic locus via allele exchange. **(D)** Quantification of the coimmunoprecipitation assay shown in A–C. Relative interaction affinity was expressed as the ratio of Psd2-HA level to Sfh4-TAP level in the IP fraction. Band intensities were measured by densitometry using ImageJ. Values represent averages from three independent experiments plotted as mean ± SEM. Statistical comparisons were performed by one-way ANOVA with Dunnett multiple comparisons test relative to the Sfh4 WT control, or by unpaired two-tailed *t* test in comparison with the Sfh4^{F175L} control (ns, not significant, $P > 0.05$; ****, $P \leq 0.0001$).

coprecipitation with Stt4 were reproducibly lower in colysis controls relative to the test (Fig. 6 B), the data leave open the formal possibility of a genuine Stt4::Psd2 interaction in vivo.

Although interpretations of the Stt4-Psd2 interaction data remain equivocal, the observed interaction was preserved when Stt4^{G1782D}-TAP was used as bait and when coprecipitations were conducted in the context of an *sfh4Δ* genetic background (Fig. 6 B). Those collective data indicate that the observed Stt4-Psd2 interaction occurred in an Sfh4-independent manner, and that an Stt4 impaired for catalytic activity remained competent for this interaction. No physical interaction was scored between Stt4-TAP and Sfh4-HA regardless of whether the coprecipitation experiment was conducted in WT or in *stt4^{G1782D}* genetic backgrounds (Fig. S5 B).

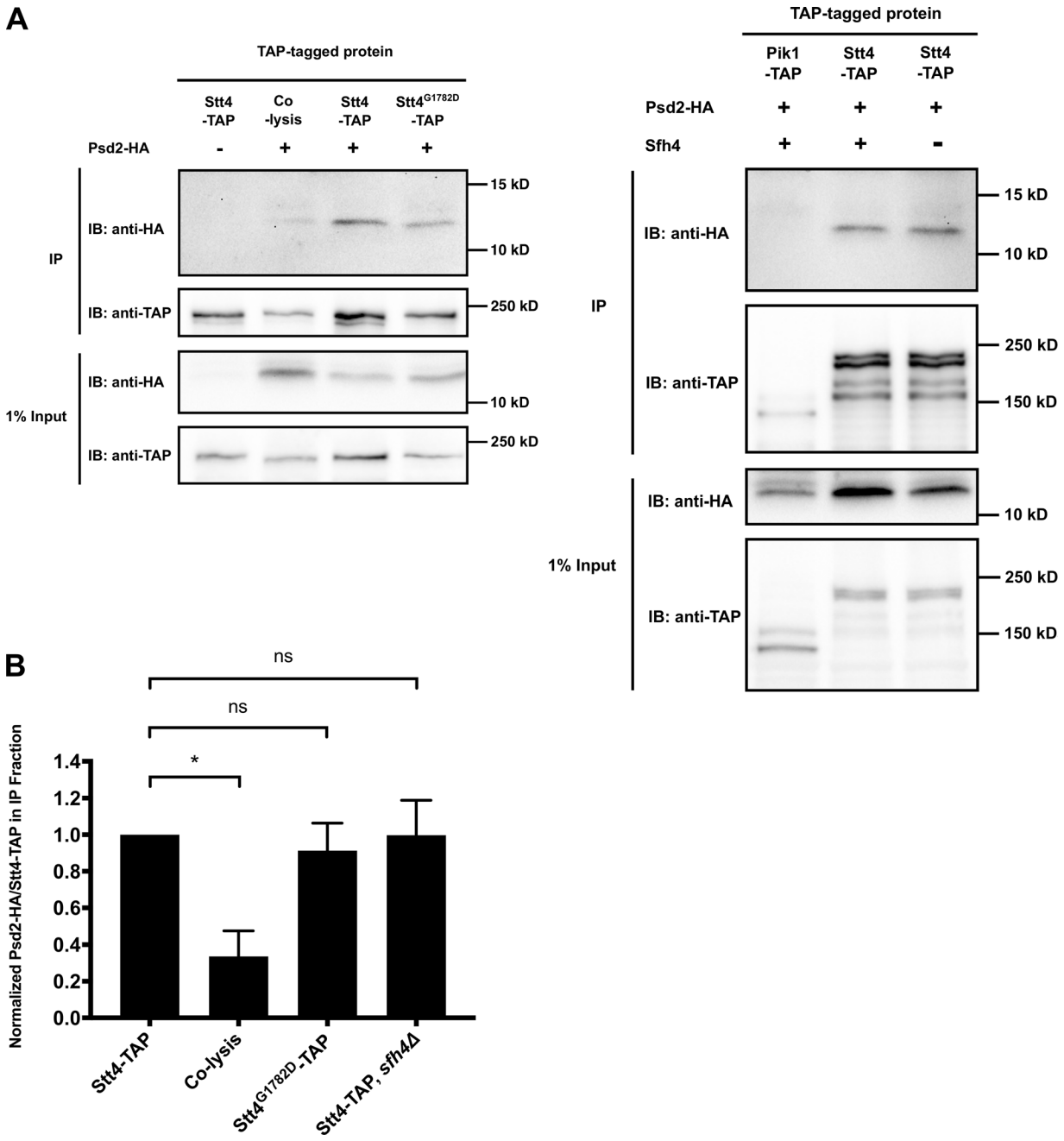

Figure 6. **Stt4 interaction with Psd2. (A)** WT or *sfh4Δ* yeast carrying integrated *STT4-TAP*, *stt4^{G1782D}-TAP*, or *PIK1-TAP* cassettes at their endogenous genomic loci (as indicated) were transformed with either a YEp(*PSD2-HA*) (+) or mock YEp vector (–), and the TAP-precipitation regimen was performed as described in Fig. 5. The colysis control is directly analogous to that described in Fig. 5 A and scores postlysis interaction of Psd2-HA and Stt4-TAP. IB, immunoblotting. **(B)** Quantification of the coimmunoprecipitation assay shown in A. Relative interaction affinity was expressed as the ratio of Psd2-HA level to Stt4-TAP level in the immunoprecipitation (IP) fraction. Band intensities were measured by densitometry with ImageJ. Values represent averages from three independent experiments plotted as mean ± SEM. Statistical comparisons were performed by one-way ANOVA with Dunnett multiple comparison test relative to the Stt4-TAP control (ns, not significant, $P > 0.05$; *, $P \leq 0.05$).

Homeostasis of PtdIns4*P* but not PtdIns(4,5)P_2 modulates Psd2 function in vivo

The Stt4 data could be interpreted as reporting a direct involvement of PtsIns4P, its downstream product PtdIns(4,5)P_2, or both phosphoinositides, in the modulation of Psd2 pathway activity in vivo. Several lines of evidence indicate that PtdIns(4,5)P_2 plays no major role in PtdSer decarboxylation by Psd2 in vivo. First, *stt4^{G1782D}* cells deficient in Psd2 activity exhibited WT targeting of the GFP-2xPH$^{PLC\delta1}$ PtdIns(4,5)P_2 biosensor to the PM, suggesting that *stt4^{G1782D}* mutants were not overtly deficient in PtdIns(4,5)P_2 homeostasis (Fig. 7 A). Second, we used an *mss4^{ts}* allele for which PtdIns(4,5)P_2 synthesis was strongly compromised, as judged by loss of PM targeting of GFP-2xPH$^{PLC\delta1}$ at 30°C (Fig. 7 B). Metabolic [^{3}H]-serine experiments demonstrated that the *mss4^{ts} psd1Δ*

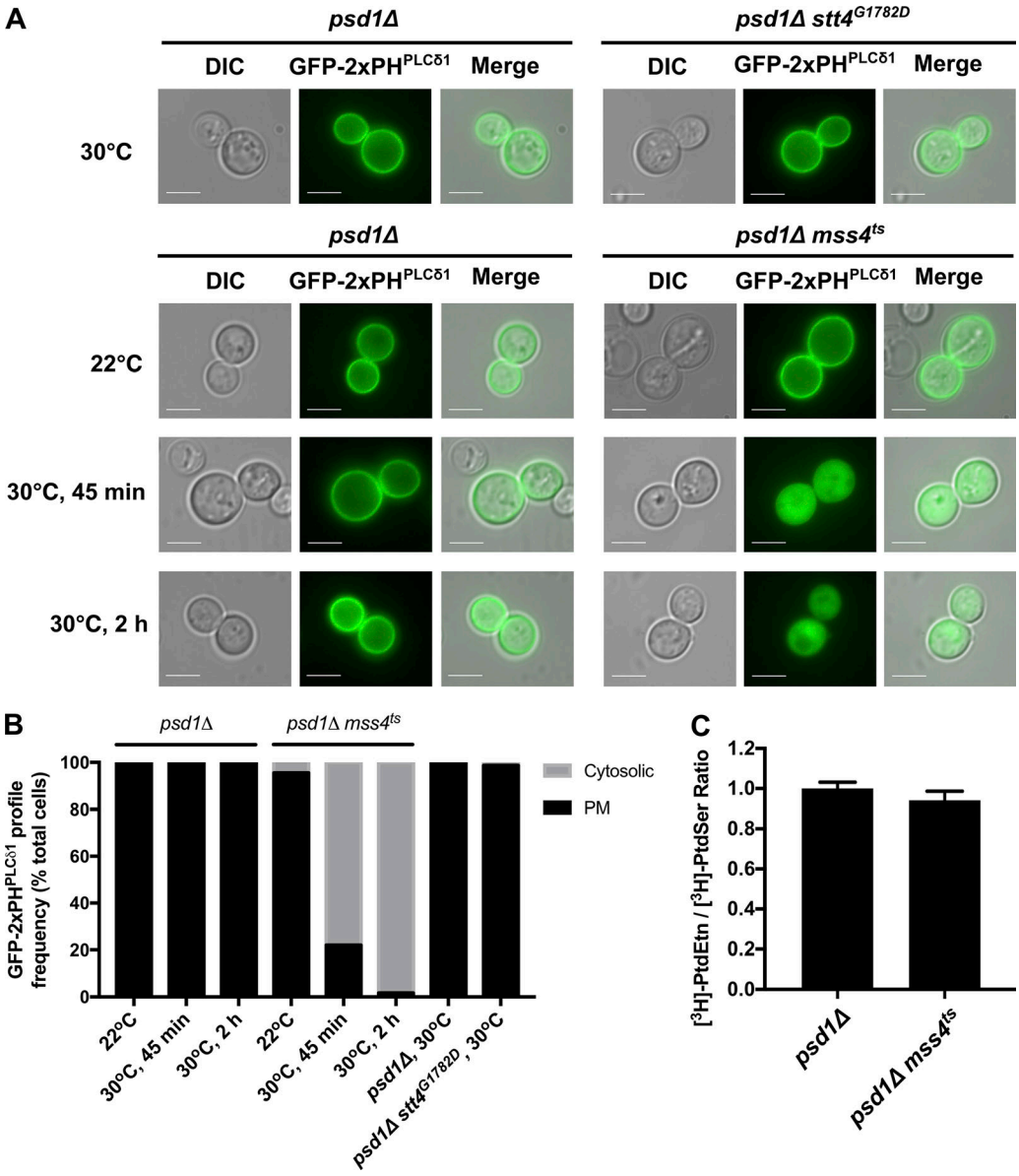

Figure 7. **Phosphoinositide specificity in activation of the Psd2 pathway. (A)** Localization of a PtdIns(4,5)P_2 biosensor is maintained in *stt4*^{G1782D} cells. Top panels: To assess the effect of reduced PtdIns4*P* synthesis on PtdIns(4,5)P_2 homeostasis, isogenic *psd1Δ* and *psd1Δ stt4*^{G1782D} cells expressing GFP-2xPH$^{PLC\delta1}$ were cultured at the permissive temperature of 30°C. Bottom panels: Cultures of isogenic *psd1Δ* and *psd1Δ mss4*^{ts} cells expressing GFP-2xPH$^{PLC\delta1}$ were grown at 22°C and shifted to 30°C for 0 min, 45 min, or 2 h as indicated (30°C is a restrictive growth temperature for the *mss4*^{ts} mutant). Genotypes are indicated at top (scale bar = 5 µm). DIC, differential interference contrast. **(B)** GFP-2xPH$^{PLC\delta1}$ PM and cytosolic localization profiles are quantified and frequencies of each class represented as percentage of total cells examined (n > 300 for each condition). **(C)** Yeast of the indicated genotype (at bottom) were cultured to midlogarithmic growth phase at 22°C and radiolabeled with [^{3}H]-serine at 30°C for 3 h. Phospholipids were extracted and quantified as described in Fig. 1 C. Conversion of PtdSer to PtdEtn is expressed as [^{3}H]-PtdEtn/[^{3}H]-PtdSer ratios for the indicated strains and related to the [^{3}H]-PtdEtn/[^{3}H]-PtdSer ratio of the isogenic *psd1Δ* control. Values represent averages from three independent experiments plotted as mean ± SEM.

double mutant was not compromised for Psd2-mediated decarboxylation PtdSer to PtdEtn under those conditions (Fig. 7 C). Thus, we conclude that PtdIns4*P* is the key phosphoinositide of relevance for Psd2 activity in vivo.

PtdIns4*P* homeostasis indirectly modulates Psd2-dependent PtdSer decarboxylation

With regard to how PtdIns4*P* homeostasis modulates Psd2 pathway activity, we made several observations that indicated an unexpectedly complex involvement of Stt4-dependent PtdIns4*P* metabolism in PtdSer decarboxylation by Psd2. The first indication came in a set of control experiments in which we observed that *psd1Δ sac1Δ* double mutants, but not *psd2Δ sac1Δ* double mutants, were Etn auxotrophs (Fig. 8 A). That is, inactivation of the Sac1 phosphatase that degrades the PtdIns4-P pool produced by Stt4 paradoxically phenocopied the effects of reduced Stt4^{G1782D} PtdIns 4-OH kinase activity in Psd1-deficient cells. This Etn auxotrophy, and its specificity for Psd1-deficient

yeast, was similarly observed in experiments in which ER-PM MCS status on the cellular PtdSer decarboxylation capacity was tested. In a first set of experiments, the *PSD1* or *PSD2* genes were deleted in a *tetherΔ* genetic background in which the structural genes for six ER-PM membrane tethers (*TCB1*, *TCB2*, *TCB3*, *SCS2*, *SCS22*, and *IST2*) are combinatorially deleted (Manford et al., 2012). In the second set of experiments, the *PSD1* or *PSD2* genes were ablated in a genetic background in which the structural genes for the Osh6 and Osh7 PtdSer/PtdIns4P transfer proteins proposed to be components of ER-PM contact sites were both deleted. Indeed, both *tetherΔ* cells and *osh6Δosh7Δ* cells recapitulated the Etn auxotrophy of $stt4^{G1782D}$ and *sac1Δ* mutants (Fig. 8 A).

What Sac1- and Stt4-deficient cells have in common is that both exhibit significantly reduced fractional contributions of PtdSer to total cellular phospholipid mass (Rivas et al., 1999; Tani and Kuge, 2014). To assess whether $stt4^{G1782D}$ similarly influences bulk cellular PtdSer levels, cells were metabolically radiolabeled with [^{3}H]-serine, lipids resolved by thin-layer chromatography (TLC), and PtdSer was collected and quantified by scintillation counting. The incorporation values obtained were normalized by culture A_{600} and expressed as a relative value to WT control. Whereas cells carrying individual *sfh4Δ*, *psd1Δ*, or *psd2Δ* mutations showed undiminished incorporation of labeled amino acid into [^{3}H]-PtdSer relative to WT, both the $stt4^{G1782D}$ and the *sac1Δ* mutants reproducibly exhibited significantly diminished incorporation (~38% of WT; Fig. 8 B). The *tetherΔ* mutant similarly showed reduced efficiencies of [^{3}H]-serine incorporation into PtdSer that were ~40% of WT cells. Whereas the *osh6Δosh7Δ* double mutant also exhibited significantly reduced [^{3}H]-serine incorporation into PtdSer, that deficit was not as large as the ones recorded for $stt4^{G1782D}$, *sac1Δ*, and *tetherΔ* mutants (Fig. 8 B). These deficits in [^{3}H]-serine incorporation into PtdSer were reflected in reduced PtdSer mass in these mutants relative to WT yeast (Fig. 8 C).

Importantly, the reductions in [^{3}H]-PtdSer synthesis for $stt4^{G1782D}$, *sac1Δ*, *tetherΔ*, and *osh6Δosh7Δ* mutants were not accompanied by decreased [^{3}H]-PtdEtn/[^{3}H]-PtdSer ratios, indicating that all of the corresponding Etn auxotrophies were manifested in the face of a Psd2 pathway fully competent for decarboxylating PtdSer molecules that engaged Psd2 to PtdEtn. This was in stark contrast to cells carrying individual *sfh4Δ*, *psd1Δ*, or *psd2Δ* cells, where [^{3}H]-PtdEtn/[^{3}H]-PtdSer ratios were decreased to ~50% of WT values (Fig. 8 D).

To test whether simple tethering of ER to the PM was sufficient to rescue PtdSer homeostasis in *tetherΔ* cells, an artificial ER-PM protein tether was expressed in the *tetherΔ* genetic background (Quon et al., 2018). Expression of this artificial staple failed to rescue [^{3}H]-PtdSer levels in *tetherΔ* yeast and failed to restore growth of *tetherΔpsd1Δ* cells in Etn-free liquid medium (Figs. 8 B and S5 C). These collective results indicated the following: (a) in agreement with the report of Storey et al. (2001), the Psd1 and Psd2 pathways contribute roughly equally to bulk cellular PtdSer decarboxylation capacity in cells using glucose as carbon source, and (b) Sfh4 deficits compromise Psd2 activity directly, whereas Stt4, Sac1, the collective MCS tethers, and the combined activities of Osh6 and Osh7 do not. Phosphoinositide mass analyses demonstrated that a common property shared by $stt4^{G1782D}$, *sac1Δ*, *tetherΔ*, and *osh6Δ osh7Δ* cells was a significant derangement in PtdIns4P homeostasis, whereas fluctuations in PtdIns(4,5)P_2 mass did not closely correlate with phenotype (Fig. 8, E–G).

PtdSer decarboxylation is primarily required for de novo PtdCho biosynthesis

The compartmental segregation of the Psd1 and Psd2 pathways suggests these two pathways address unique cellular (compartment-specific?) PtdEtn requirements. Whereas we employed Etn auxotrophy in this study as phenotypic readout for Psd2 pathway activity, PtdSer metabolism also affects PtdCho biosynthesis (Boumann et al., 2006; Storey et al., 2001). The de novo pathway for PtdCho biosynthesis uses PtdEtn as precursor which, via a series of three headgroup methylation reactions, is converted to PtdCho. As the Etn-free medium used throughout this study were also choline deficient, contributions of PtdSer decarboxylation to de novo PtdCho synthesis could be assessed by addition of choline (rather than Etn) to the medium.

Indeed, supplementation of Etn-free growth medium with a low concentration of choline (10 µM) was sufficient to partially rescue the growth defects of *psd1Δsfh4Δ* and of *psd1Δpsd2Δ* double mutants (Fig. S5, D and E). Notably, the Etn-prototrophy of these mutants in choline-supplemented medium required a functional pathway for sphingosine-phosphate degradation to Etn-phosphate catalyzed by the *DPL1* gene product. Even 100 µM choline was insufficient to rescue growth of these mutants in a *dpl1Δ* genetic background (Fig. S5 D). Those data indicated that PtdSer decarboxylation in yeast primarily supports de novo PtdCho biosynthesis and sharpen previous findings that the Etn-auxotrophy of *psd1Δpsd2Δ* double mutants is rescued in a Dpl1-dependent manner by excessive choline (Storey et al., 2001).

Strikingly, low choline (10 µM) supplementation was significantly more efficient in rescue of the growth defects of $psd1\Delta stt4^{G1782D}$, *psd1Δsac1Δ*, *tetherΔpsd1Δ*, and *osh6Δosh7Δpsd1Δ* cells relative to the rescue scored for *psd1Δsfh4Δ* and *psd1Δpsd2Δ* double mutants. In those cases, the efficiencies of rescue were similar to those observed when growth medium was supplemented with 2 mM Etn (Fig. S5, D and E). These data again indicate that the contribution of Stt4-dependent PtdIns4P homeostasis to Psd2-mediated PtdEtn production is mechanistically distinct from the functional involvement of Sfh4.

Discussion

The proposed ER-endosomal MCS that organizes Psd2-mediated decarboxylation offers an attractive experimental model for testing basic concepts that are presumed to apply generally to MCS biology. The uniqueness of this system lies in the fact that the proposed functional properties of this candidate MCS can be interpreted in terms of a clear physiological context (Voelker, 2005). The current Psd2 ER-endosomal MCS model rests on two lines of evidence. First, genetic evidence identifies Sfh4 and Stt4 as important components, as deficiencies in either function compromise Psd2 activity in vivo (Trotter et al., 1998; Wu et al., 2000). These data do not speak to whether the involvements of

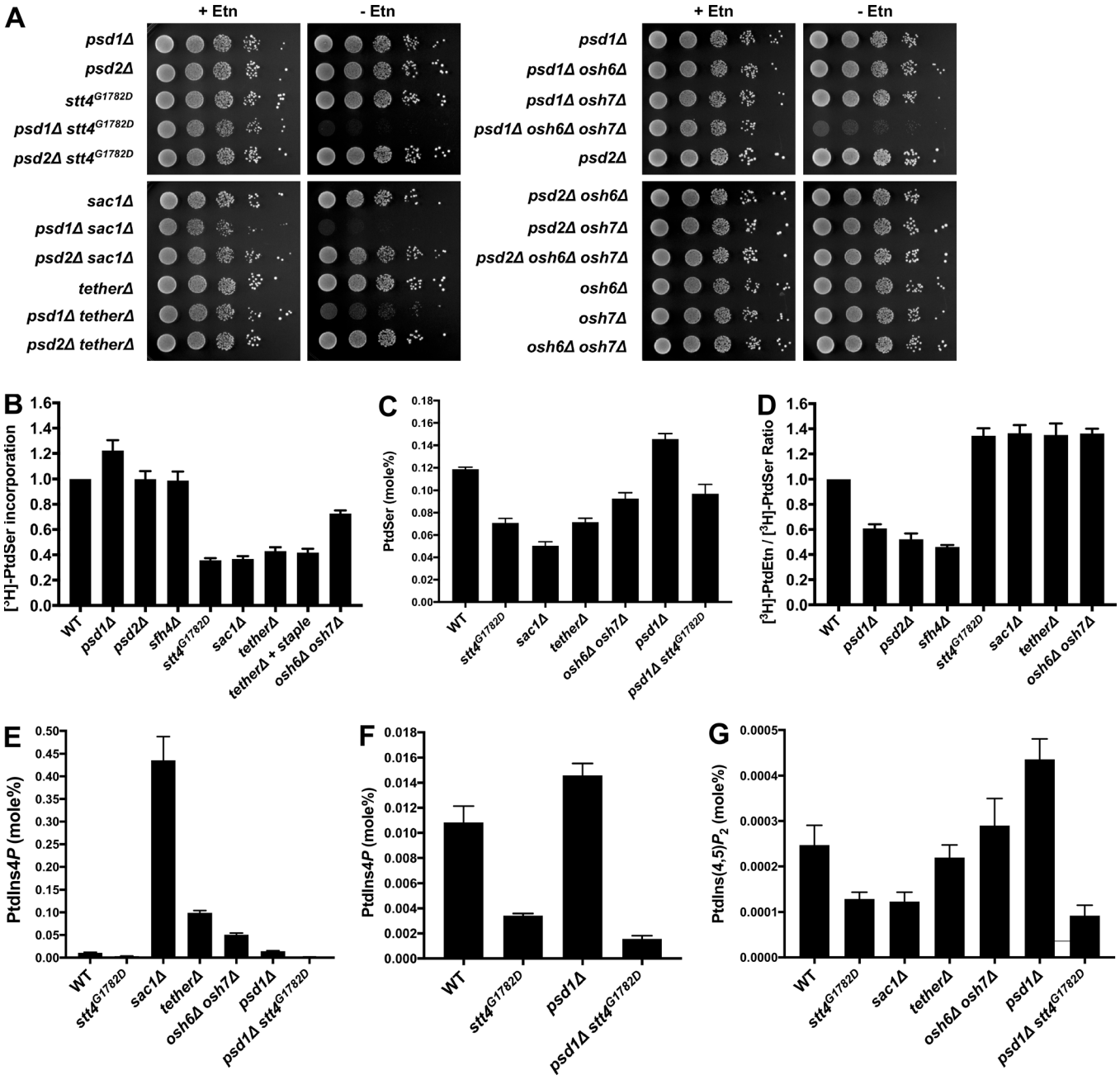

Figure 8. **Complex relationship between PtdIns4*P* and PtdSer homeostasis and Psd2 activity in vivo. (A)** Isogenic yeast strains with the designated genotype were spotted in 10-fold dilution series on glucose minimal medium with or without Etn supplementation (2 mM) as indicated. Plates were incubated at 30°C for 72 h. **(B)** Yeast strains of the indicated genotype were labeled with [^{3}H]-serine for 3 h, and [^{3}H]-PtdSer produced was resolved by TLC, scraped, and quantified by scintillation counting. Total [^{3}H]-PtdSer cpm for each strain was normalized by A_{600} and related to the normalized [^{3}H]-PtdSer level of WT cells analyzed in the same experiment (set at 1.0). Staple refers to expression of the artificial ER-PM tether. Values represent averages from at least three independent experiments and are plotted as mean ± SEM. **(C)** Quantification of PtdSer in the indicated yeast strains. Data for each species are presented as mol% after normalizing to total phospholipids in each sample. Values represent averages from four biological replicates plotted as mean ± SEM. **(D)** Yeast strains were labeled with [^{3}H]-serine for 3 h, and the efficiency of PtdSer decarboxylation to PtdEtn was determined by TLC separation followed by scintillation counting. The conversion of PtdSer to PtdEtn was expressed as the [^{3}H]-PtdEtn/[^{3}H]-PtdSer ratios of the indicated strains and related to the [^{3}H]-PtdEtn/[^{3}H]-PtdSer ratio of the WT control analyzed in the same experiment. Values represent averages from at least three independent experiments and are plotted as mean ± SEM. **(E and F)** Quantification of PtdIns4*P* in the indicated yeast strains. Data for each species are presented as mol% after normalizing to total phospholipids in each sample. **(F)** Magnified scale of PtdIns4*P* values for the indicated strains from E. **(G)** Quantification of PtdIns(4,5)P_2 in the indicated yeast strains. For E–G, the values represent averages from four independent biological replicates plotted as mean ± SEM (except for the *sac1Δ* strain, where $n = 3$).

Sfh4 and/or Stt4 in the Psd2 pathway report direct or indirect effects. A second line of supporting biochemical evidence consists of an unvalidated chain of protein::protein interactions that connect Psd2 with Sfh4, the functionally uncharacterized Pbi1, and known MCS tethers of the VAP family (Scs2 and Scs22) that bind Stt4 (Riekhof et al., 2014).

Herein, we show that the Sfh4 PITP and the Stt4 PtdIns 4-OH kinase are required for biologically sufficient activation of Psd2 via a mechanism that (a) requires Stt4 enzymatic activity and (b) employs Sfh4 in what we describe as a noncanonical fashion that is independent of its lipid transfer activity but obligatorily requires Sfh4 to complex with Psd2. Indeed, the data identify Sfh4 as the only component other than Psd2 that can be confidently assigned as being directly involved in the yeast Psd2 pathway. The cumulative results report a substantially indirect role for Stt4 in regulating Psd2 activity. We presently favor a model where Stt4 mediates its effects indirectly through PtdIns4*P* responsive control of bulk PtdSer synthesis and/or targeting of Psd2 to the correct intracellular compartments (Fig. 9). Taken together, the data fail to support the foundational tenets of the Psd2 MCS model as proposed.

Reevaluation of the existing Psd2 MCS model

Using genetic and metabolic tracer analyses, we find that neither the uncharacterized Pbi1 nor the MCS tethers Scs2 and Scs22 play any discernible role in regulating PtdSer decarboxylation by Psd2 in vivo. Similarly, neither functional ablation of each individual *OSH* gene, structural genes encoding other tethers (Vps13, Lam5, and Lam6), nor individual overexpression of the purported PtdSer transfer proteins Osh6 and Osh7, had any significant biological consequences for Psd2 activity. Taken together, these collective data report that neither Scs2/Scs22, Pbi1, Vps13, Lam5, Lam6, nor any individual member of the yeast *OSH* protein family, is a quantitatively significant regulator of Psd2 activity, at least not under laboratory conditions. Sfh4, Stt4 and, paradoxically, Sac1 represent the only individual components for biologically sufficient Psd2-mediated PtdSer decarboxylation in cells.

A noncanonical role for a PITP in regulating lipid metabolism

Given established roles of PITPs in stimulating PtdIns 4-OH kinase activities in vivo (Bankaitis et al., 2010; Schaaf et al., 2008; Xie et al., 2018), we expected Sfh4 to employ its PtdIns-binding activities to potentiate Stt4 activity for production of a local PtdIns4*P* pool required for Psd2 activity. While our demonstration that *stt4*^{G1782D} encodes a crippled enzyme with reduced PtdIns 4-OH kinase activity in vivo is consistent with this scenario, other data reject such a simple interpretation. Most notable are the demonstrations that the PtdIns-binding/exchange activities of Sfh4 (and therefore its ability to stimulate PtdIns 4-OH kinase activity) were dispensable for Psd2 activation, and that Sfh4 activities in PtdIns-binding/exchange could be cleanly uncoupled from those required for promoting Psd2-dependent PtdSer decarboxylation. Indeed, when viewed in the context of the six yeast Sec14-like PITPs, the specific ability of Sfh4 to stimulate Psd2 activity can now be accounted for by the unique ability of Sfh4 to physically interact with Psd2 in vivo. The

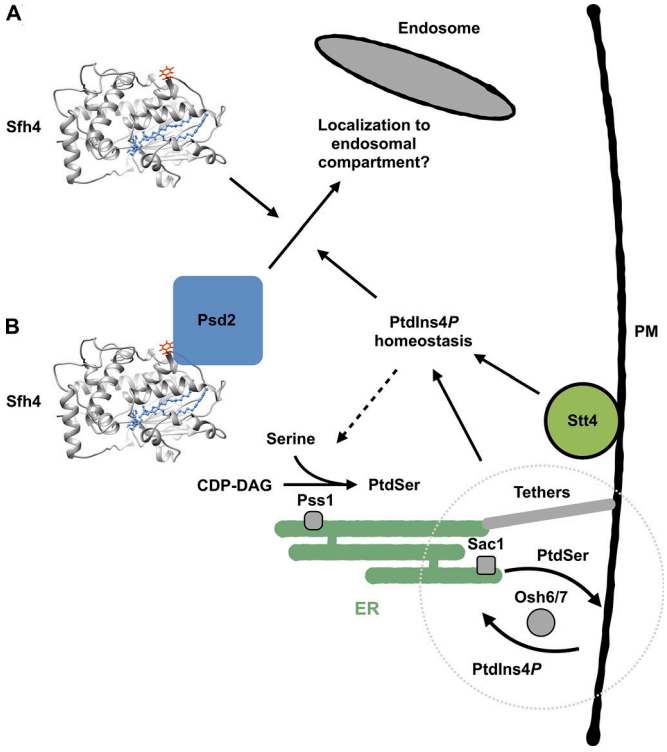

Figure 9. **Sfh4 and Stt4 regulate Psd2 via distinct mechanisms. (A and B)** Sfh4 directly modulates Psd2 activity by entering into a physical association with Psd2, where it functions as either a trafficking chaperone that guides Psd2 to what is most likely an endosomal compartment (A), or a noncatalytic subunit required for Psd2 catalytic activity (B). These two possibilities are not mutually exclusive. By contrast, Stt4 generates a PM pool of PtdIns4*P*, the homeostasis of which is essential for proper targeting of Psd2::Sfh4 to the correct compartment. Reduced Stt4 activity, inactivation of the Sac1 PtdIns4*P* phosphatase, or disruption of PM-ER tethers (including Osh6/Osh7) results in deranged PtdIns4*P* homeostasis with the result that Psd2 is mislocalized and/or PtdSer synthesis in the ER is compromised.

functional relevance of this interaction is convincingly demonstrated by the fact that the graded biochemical defects in the Sfh4:Psd2 interaction represented in an allelic series of Sfh4 variants are proportionately reflected in the severities of Psd2-dependent PtdSer decarboxylation defects exhibited by cells reconstituted for expression of those variants as sole sources of Sfh4.

While it remains formally possible that the residual low-level PtdIns-exchange activities of the Sfh4^{T266D,K269A} and Sfh4^{T266W,K269A} PtdIns-binding mutants might be sufficient to stimulate Stt4 activity in the close quarters of some Psd2-Sfh4-Stt4 complex, the available data do not support the case that Psd2 enzymatic activity is directly stimulated by PtdIns4*P* (see below). Rather, the data are most consistent with Sfh4 serving as a scaffold required for Psd2 activation. Such a scaffolding function could serve to activate the decarboxylase in a noncatalytic subunit capacity (Fig. 9). An interesting possibility inherent in this scenario is that differential lipid-binding states of Sfh4 might serve as regulatory inputs for control of Psd2 catalytic activity. Alternatively, the Sfh4::Psd2 interaction might play a key role in ensuring the targeting of the decarboxylase to the appropriate intracellular compartment (Fig. 9).

MCS tethers and homeostasis of Stt4-dependent PtdIns4*P* pools

Whereas a productive Sfh4::Psd2 interaction is physiologically relevant, the genetic evidence for Stt4 involvement in Psd2 activity remains difficult to interpret given the lack of in vivo data functionally validating the observed Psd2::Stt4 interaction. While we report a statistically significant Sfh4-independent Psd2::Stt4 physical interaction that was not diminished by compromise of Stt4 catalytic activity, the physiological authenticity of this interaction remains uncertain. The major caveat is that detectable postlysis association of Psd2 and Stt4 was reproducibly observed in control experiments, the statistical significance of the interaction notwithstanding. However equivocal, these results leave open the formal possibility that Psd2 and Stt4 also engage in a dedicated complex required for biologically sufficient Psd2 activity in vivo. As Stt4 catalytic deficiencies apply to all Stt4 pools, and not just to some potential Psd2-bound Stt4 pool, the phenotypic data collected from *stt4*^{G1782D} mutants would sum both direct and indirect effects of Stt4 activity and PtdIns4*P* homeostasis on Psd2 activity.

On balance, we favor the interpretation that Stt4 plays a primarily (and perhaps exclusively) indirect role in modulating the Psd2 pathway in cells (Fig. 9). The bulk of the supporting evidence to that effect comes from our demonstration that *stt4*^{G1782D} cells, *sac1Δ* cells, *tetherΔ* mutants, and *osh6Δ osh7Δ* double mutants all evoked Etn (and Cho) auxotrophies in *psd1Δ* genetic backgrounds. Critically, these did so without affecting the efficiencies with which the PtdSer molecules that had entered the Psd2 pathway were decarboxylated. These disparate genetic backgrounds share two common features. First, bulk PtdSer synthesis was significantly reduced in *stt4*^{G1782D}, *sac1Δ*, *tetherΔ*, and *osh6Δ osh7Δ* cells. Second, *stt4*^{G1782D}, *sac1Δ*, *tetherΔ*, and *osh6Δ osh7Δ* mutants all exhibited significant derangements in PtdIns4*P* homeostasis. We show herein that (a) production of this phosphoinositide is reduced in *stt4*^{G1782D} yeast, (b) PtdIns4*P* is elevated in *osh6Δ osh7Δ* mutants, and (c) in agreement with previous reports (Guo et al., 1999; Manford et al., 2012; Rivas et al., 1999; Stefan et al., 2011), PtdIns4*P* accumulates to high levels in *sac1Δ* and *tetherΔ* mutants.

PtdIns4*P* homeostasis and Psd2 function

The most parsimonious explanation of these results is that perturbed PtdIns4*P* homeostasis (either PtdIns4*P* deficit or excess) interferes with bulk PtdSer synthesis (Fig. 9) and that the Psd2 pathway is particularly sensitive to reductions in the substrate pool. Several potential mechanisms account for such pathway-selective sensitivity to reduced PtdSer synthesis. One possibility is that the compartment of Psd2 residence presents a membrane environment with an intrinsically limited accessibility to PtdSer, a deficit that is exacerbated under conditions of reduced synthesis of bulk PtdSer. Given recent evidence that Psd1 is localized to both mitochondria and ER (i.e., the site of PtdSer synthesis; Friedman et al., 2018), it is plausible that Psd1 has more direct access to newly synthesized PtdSer than does Psd2. Alternatively, given the recognized role of PtdIns4*P* as regulator of Golgi and endosomal membrane trafficking (Bankaitis et al., 2010; Graham and Burd, 2011; Wang et al., 2019), a likely consequence of derangements in PtdIns4*P* homeostasis would be Psd2 missorting to compartments whose membrane environments might be particularly hostile to biologically sufficient Psd2 activity under conditions of reduced PtdSer synthesis (Fig. 9).

Distinguishing between these possibilities demands that the intracellular localization of Psd2 be assigned at high resolution, followed by determination of whether localization of the enzyme is altered in the face of Sfh4 deficiencies or of deranged PtdIns4*P* homeostasis. Unfortunately, in our hands, using multiple approaches, the low cellular abundance of Psd2 frustrated attempts to assign a precise compartmental localization to the endogenous protein. In those experiments, we failed to reproduce the results of Gulshan et al. (2010) that claimed endogenous Psd2 targets to endosomes. We could neither detect endogenous Psd2 in a variety of strains we generated, nor could we detect Psd2 in the same strains published by Gulshan et al. (2010). Whereas overexpressed Psd2 localized to cytosolic puncta in a pattern consistent with what Gulshan et al. (2010) claimed represented endogenous Psd2, those puncta colocalized with endosomal markers in only ∼2% of the cells imaged. Moreover, neither cellular Sfh4 nor Stt4 status affected those localization profiles. Unfortunately, the level of Psd2 overexpression required to visualize the enzyme also relieved cells of the Sfh4 requirement for biologically sufficient Psd2 activity. We therefore cannot confidently interpret those results. In our view, while an endosomal location for Psd2 seems likely, the precise compartmental location for endogenous Psd2 remains unresolved.

Lipid transfer proteins and MCS function

Finally, the proposed Psd2 MCS model was not buttressed by any imaging data that would suggest the enzyme is localized at sites of close organelle apposition, in contrast to other MCS where convincing imaging data are available (Shai et al., 2018; Valm et al., 2017; Wu et al., 2018). Nonetheless, the results reported herein translate to other MCS systems in that these highlight the complexities associated with interpreting the types of data generally used to construct mechanistic cartoons for MCS function. As one example, the noncanonical mechanism for PITP function described in this study emphasizes that caution be exercised in interpreting the functions of MCS-associated proteins that show lipid-transfer activities in vitro. MCS typically include at least one such component, and it is generally assumed, in the absence of direct in vivo evidence, that such lipid-transfer activities translate to MCS-associated interorganelle lipid-transfer in living cells. The indirect involvements of Stt4 and MCS tethers, in the face of genetic and/or interaction data that could otherwise be construed to argue for direct involvements, provide a second cautionary example. The third example is the lipid droplet:nuclear/vacuole junction-associated PtdIns/ergosterol exchange protein Sfh3 (Eisenberg-Bord et al., 2018; Teixeira et al., 2018; Tripathi et al., 2019). Sfh3 uses its lipid binding/exchange activity to inhibit lipid mobilization from lipid droplets in vivo (Ren et al., 2014), a mode of action that diverges from popular models for how lipid transfer proteins function in MCS contexts. We suggest that the idea that MCS are

involved in organizing lipid synthesis, rather than prosecuting intermembrane lipid transport, deserves more serious consideration than is afforded to it in contemporary literature. In sum, this study emphasizes the need for direct and physiologically relevant assays for confident mechanistic dissection of MCS function.

Materials and methods

Yeast strains, plasmids, primers, and reagents

Yeast strains are described in Table S2, plasmids are listed in Table S3, and a comprehensive list of the primers used in this study is provided in Table S4. All phospholipids were from Avanti Polar Lipids, and restriction endonucleases were from New England Biolabs. All other standard reagents were obtained either from Sigma-Aldrich or Thermo Fisher Scientific.

[^{3}H]-serine metabolic radiolabeling and phospholipid analysis

Strains were grown in uracil-free minimal medium containing 3% glucose and 2 mM Etn to late-log phase at 30°C with shaking. Cultures were diluted to an A_{600} = 0.3 and supplemented with 3.33 µCi/ml L-[^{3}H]-serine (ART 0246; American Radiolabeled Chemicals) and incubated for an additional 3 h at 30°C with shaking. Incorporation of radiolabel was terminated by addition of ice-cold trichloroacetic acid (5% final concentration), and samples were incubated on ice for 30 min. Cell pellets were washed twice with cold ddH_2O, resuspended in 1.5 ml ddH_2O:absolute ethanol (1:4, vol/vol), and incubated at 100°C for 45 min. The lipids were then extracted from the 1:4 water:ethanol mixture by adding 4 ml of $CHCl_3$, 4 ml of methanol, and 3.3 ml of 0.2 M KCl, with shaking, and centrifuging at top speed to separate the phases. The organic phase was collected and washed twice with 7.6 ml of the practical upper phase (PBS:methanol, 9:10, vol/vol), saturated with $CHCl_3$), and dried under a stream of N_2 gas, and the lipid film was resuspended in $CHCl_3$/CH_3OH (2:1, vol/vol) charged with 1 mg/ml butylated hydroxytoluene. Lipids were resolved by Silica Gel H TLC (Analtech) in a $CHCl_3$/2-propanol/0.25% KCl/triethylamine (30:9:6:18, vol/vol/vol/vol) solvent system. After development, plates were sprayed with 0.2% (wt/vol) 8-anilino-1-naphthalenesulfonic acid, and lipids were visualized under UV illumination. Individual lipid species were identified using internal standards (Avanti) and collected by scraping. Radioactivity was quantified by liquid scintillation counting.

Phosphoinositide quantifications

To quantify PtdIns4*P* using a metabolic labeling/TLC procedure, yeast strains were grown overnight in uracil-free minimal medium containing 3% glucose and 1% casamino acids (223050, BD) and offered 10 µCi/ml [^{3}H]*myo*-inositol (ART 0116A; American Radiolabeled Chemicals). After an incorporation window of ≥20 h, labeling was terminated with trichloroacetic acid (5% final concentration), and samples were incubated on ice for 30 min. Cells were pelleted (16,000 *g* for 1 min), washed twice in 500 µl of cold ddH_2O, and resuspended in 500 µl of 4.5% perchloric acid. Approximately 300 µl of 0.5-mm glass beads were added, and cells were disrupted by vigorous agitation for 10 min in 1-min bursts with 1-min rest intervals on ice. Lysates from disrupted cells were collected and centrifuged at 16,000 *g* for 10 min, and the pellet was washed with 500 µl of 100 mM EDTA (pH 7.4) and resuspended in 500 µl of $CHCl_3$/CH_3OH/HCl (2:1:0.007). A two-phase separation was produced by addition of 100 µl of 0.6 M HCl, and samples were vortexed for 5 min and centrifuged for 5 min (16,000 *g*). The organic phase was collected, washed twice with 250 µl of CH_3OH/0.6 M HCl/$CHCl_3$ (1:0.94:0.06), dried under N_2 gas, and resuspended in 50 µl $CHCl_{33}$. Samples were resolved by TLC on Partisil LK6DF 60-Å silica gel plates (Whatman, 4866-821) using a $CHCl_3$/CH_3OH/ddH_2O/NH_4OH (1:0.83:0.15:0.1) solvent system. Radiolabeled lipids were visualized by autoradiography.

Total phosphoinositide mass profiles were determined by anion exchange chromatography of deacylated lipid species. Lipids were extracted under acidic conditions to increase recovery of phosphoinositides from yeast cells (Kanehara et al., 2015). In brief, cells were homogenized in extraction solvent containing chloroform/methanol/concentrated HCl (100:100:0.7) and centrifuged. Clarified supernatant was transferred to a fresh tube. The extractions were repeated once, and the lipid extracts were pooled. The lipid extracts were washed three times with washing solvent containing chloroform/methanol/0.6 N HCl (3:48:47), and the lower organic phases were transferred to a new tube. The washed extracts were dried, and phosphoinositides were deacylated with methylamine reagent containing methanol/40% methylamine in water/1-butanol/water (47:36:9:8) at 50°C for 45 min. The aqueous phases were dried and resuspended in 1-butanol/petroleum ether/ethyl formate (20:40:1). Deacylated phosphoinositides were then extracted twice using MilliQ water, dried, and resuspended in water for analysis on the (ICS)-5000 ion chromatography system (Dionex). Phosphoinositide levels were calculated based on external calibration curves constructed using known concentrations of phosphoinositide standards.

Phospholipids were analyzed by liquid chromatography/mass spectrometry. In brief, phospholipids were separated on a Phenomenex Luna Silica 3-µm column (internal diameter 150 × 2.0 mm; Lu et al., 2019). Individual polar lipid species were quantified by referencing to spiked internal standards including PtdCho (14:0/14:0), PtdEtn (14:0/14:0), d31-PtdSer (16:0/18:1), PtdSer (17:0/20:4), PtdOH (17:0/17:0), PtdOH (17:0/20:4), and phosphatidylglycerol (14:0/14:0) obtained from Avanti Polar Lipids. PtdIns (8:0/8:0) was also included (Echelon Biosciences).

Fluorescence imaging

Yeast cultures for GFP-2xPH^{Osh2} and GFP-2xPH$^{PLC\delta1}$ imaging were grown in synthetic defined medium lacking uracil at either 30°C or 25°C with shaking to midlogarithmic growth phase. Cells were collected at 25°C by centrifugation at 5,000 *g* for 1 min and resuspended into fresh uracil-deficient medium before analysis. Cells were sealed under a coverslip coated with Concanavalin A (Sigma-Aldrich) and examined at 25°C. The imaging system employed a CFI plan Apochromat Lambda 100× NA 1.45 oil-immersion objective lens mounted on a Nikon Ti-U microscope base (Nikon) interfaced to a Photometrics CoolSNAP HQ2 high-sensitivity monochrome charge-coupled device camera (Roper Scientific) or an Andor Neo sCMOS charge-coupled device camera (Andor Technology). A Lumen 200 Illumination

System (Prior Scientific) was used in conjunction with a B-2E/C (465–495 nm/515–555 nm; excitation/emission) filter set (Nikon). Images were captured using NIS Elements software package (Nikon, version 4.10).

Homology modeling

Structural models of Sfh4 were generated with MOE 2013.08 Modeling package. The target Sfh4 sequence was aligned to the PtdIns-bound Sfh3 structure (PDB: 4J7Q; 1.55-Å resolution) with a sequence similarity of ∼66%. PtdIns ligand was included in the environment to generate induced fit homology models of Sfh4-PtdIns complex. By default, 10 independent intermediate models were generated. These different intermediate homology models were generated as a result of permutational selection of different loop candidates and side chain rotamers. The intermediate model, which scored best according to the selected force field (Amber99), was chosen as the final model and was subjected to further optimization.

Protein purification

pET28b plasmid derivatives programming expression of the appropriate recombinant proteins were transformed into BL21 *E. coli* (DE3; New England BioLabs). Recombinant proteins of interest were bound to TALON metal affinity beads (Clontech), eluted with imidazole (gradient 10–200 mM), and dialyzed (68100, Thermo Fisher Scientific). In the case of Sec14, dialysis was against 300 mM NaCl, 25 mM Na_2HPO_4 (pH 7.5), and 5 mM β-mercaptoethanol. Purified Sfh4 proteins were dialyzed against the same buffer with the exception that 50 mM Na_2HPO_4 was used. Protein mass was quantified by SDS-PAGE using BSA standards and A_{280} measurements.

PtdIns-transfer assays

Purified recombinant proteins were preincubated in the presence of [^{3}H] *myo*-inositol labeled acceptor membranes, in buffer (300 mM NaCl and 25 mM Na_2HPO_4, pH 7.5) for 30 min at 37°C before initiating the assay by addition of radiolabeled donor membranes (Bankaitis et al., 1990; Schaaf et al., 2008).

Real-time fluorescence dequenching PyrPtdIns-transfer assays

Measurements of protein-mediated PyrPtdIns-transfer activity from donor vesicles (with TNP-PtdEtn quencher) to acceptor vesicles (without TNP-PtdEtn quencher) were conducted using a real-time fluorescence dequenching assay (Grabon et al., 2017; Huang et al., 2016; Somerharju et al., 1987). For the acceptor vesicles, stock solutions of egg PtdCho and egg phosphatidic acid were mixed in a 291/9 nmol (97/3 mol%) ratio and dried under nitrogen gas. The resulting lipid film was then hydrated with 2 ml of low-phosphate buffer (25 mM Na_2HPO_4 and 300 mM NaCl, pH 7.5) and sonicated on ice for 10 min. For donor vesicles, stock solutions of egg PtdCho, PyrPtdIns, and TNP-PtdEtn were combined in a 4/0.5/0.5 nmol ratio. After the solvent was evaporated, the lipid film was resuspended in 10 µl ethanol, and the solution was injected into the buffer system containing the acceptor vesicles. After a 5- to 10-min equilibrium period, the fluorescence intensity (excitation 346 nm; emission 378 nm) was recorded as a function of time at 37°C using an ISS K2 fluorimeter. To titrate PtdIns-transfer activities, 1-µg aliquots of purified recombinant protein were serially injected into assay mixtures at 250-s time intervals (five injections total).

Western blot analysis

Samples were boiled, and individual proteins were resolved by SDS-PAGE. After transfer, the PVDF membranes were decorated with the following primary antibodies: anti-HA antibody (BioLegend 901501, mouse), anti-TAP antibody (Invitrogen CAB1001, rabbit), anti-tubulin antibody (Abcam ab184970, rabbit), and anti-Sfh4 antibody (Bankaitis laboratory, Texas A&M University, rabbit). The blots were subsequently developed using the following HRP-conjugated secondary antibodies: goat anti-mouse IgG antibody (Millipore AP124P) and goat anti-rabbit IgG antibody (Millipore AP307P). Immunoblot images were acquired using Bio-Rad ChemiDoc XRS+ system. Relative band intensities on the blots were quantified using ImageJ (version 1.51s, National Institutes of Health).

Coimmunoprecipitation experiments

All assays were performed using lysed spheroplasts (Gulshan et al., 2010). Cultures (100 ml) were grown to early log phase at 30°C with shaking. Cells were collected by centrifugation and washed in spheroplast solution I (1 M sorbitol, 10 mM $MgCl_2$, 50 mM K_2HPO_4, 30 mM DTT, and 1 mM PMSF). Cells were then resuspended in spheroplast solution II (1 M sorbitol, 10 mM $MgCl_2$, 50 mM K_2HPO_4, 30 mM DTT, 1 mM PMSF, 25 mM sodium succinate, and 250 U/ml lyticase) and incubated at 37°C for 15–30 min on a shaker at 100 rpm.

Spheroplasts were collected by centrifugation and disrupted in lysis buffer (1% Triton X-100, 0.15 M NaCl, 50 mM Tris-HCl, 2 mM EDTA, 200 µM sodium vanadate, 1 mM PMSF, and protease inhibitor tablets) with vigorous vortexing with 0.5-mm glass beads. Cell-free extracts were clarified by centrifuging lysates at 20,000 *g* for 5 min. Supernatants were collected, and lysate protein concentrations were determined by BCA assay for purposes of normalization. For immunoprecipitation, cell lysates (∼12 mg total protein) were incubated with anti-TAP antibody (Invitrogen CAB1001, rabbit) for 4 h at 4°C. Complexes were captured by addition of Protein A/G-magnetic beads (Thermo Fisher Scientific, Pierce Protein A/G Magnetic beads, 88802) reconstituted in lysis buffer to the samples, followed by incubation for 2 h at 4°C. Protein A/G-magnetic beads were subsequently recovered on a magnetic field stand and washed four times in wash buffer (0.15 M NaCl, 50 mM Tris-HCl, 2 mM EDTA, 200 µM sodium vanadate, 1 mM PMSF, and protease inhibitor tablets). Bound complexes were eluted from the beads by adding Laemmli buffer and heating. Precipitated materials were resolved by SDS-PAGE and immunoblotted with anti-HA antibody (BioLegend 901501, mouse) and anti-TAP antibody (Invitrogen CAB1001, rabbit). Immunoblot images were acquired using Bio-Rad ChemiDoc XRS+ system.

Statistical analysis

All statistical analyses were performed using GraphPad Prism software with either unpaired two-tailed *t* test or one-way

ANOVA with Dunnett multiple comparisons test (ns, $P > 0.05$; *, $P \le 0.05$; **, $P \le 0.01$; ***, $P \le 0.001$; ****, $P \le 0.0001$). The normality of the data was examined by Shapiro–Wilk test.

Online supplemental material

Fig. S1 documents the consequences of functional modulation of individual tethers and Osh proteins on Psd2 pathway activity and outlines the design of the synthetic gene array screen developed to identify nonessential genes required for Psd2 activation in vivo. Fig. S2 documents the results of phenotypic assays for Psd2 activity in cells bearing *stt4* mutations, overexpressing individual Stt4 subunits, or lacking the single nonessential Sfk1 subunit. Fig. S3 shows that Sfh4 is the one yeast Sec14-like PITP required for in vivo Psd2 activity, shows a homology model of the Sfh4 structure with the PtdIns-binding motif, validates the biochemical properties of PtdIns-binding barcode mutants defective in PtdIns binding and transfer, and shows documents that the Sfh4 and Stt4 requirements for Psd2 activation in vivo are not bypassed by defects in phosphoinositide phosphatases. Fig. S4 describes the mutagenic PCR screen for isolation of *sfh4* mutants specifically defective in Psd2 activation in vivo and their biochemical characterization. Fig. S5 describes data indicating no role for Pik1 in Psd2 pathway activity and the Etn and Cho auxotrophies of mutants with the indicated genotypes. Table S1 lists the results of the synthetic genetic array screen for the loss-of-function mutations that deactivate Psd2 in vivo. Table S2, Table S3, and Table S4 list the yeast strain genotypes, plasmids, and primers used in this study, respectively.

Acknowledgments

V.A. Bankaitis dedicates this work to the memory of the incomparable Lina Obeid.

We are grateful to W. Scott Moye-Rowley (Department of Molecular Medicine, University of Iowa, Iowa City, IA) for his generous gifts of yeast strains and plasmids and for his helpful discussions regarding Psd2 localization experiments. This work was supported by grants from the National Institutes of Health (R35 GM131804) to V.A. Bankaitis. The M. Schuldiner laboratory is supported by the Deutsche Forschungsgemeinschaft (SFB1190; Compartmental gates and contact sites) and a Volkswagen Foundation Life grant. M. Schuldiner is an incumbent of the Dr. Gilbert Omenn and Martha Darling Professorial Chair in Molecular Genetics. M. Eisenberg-Bord is supported by a PhD fellowship from the Azrieli Foundation.

The authors declare no competing financial interests.

Author contributions: Conceptualization: Y. Wang, P. Yuan, A. Tripathi, V.A. Bankaitis; Investigation: Y. Wang, P. Yuan, A. Grabon, A. Tripathi, D. Lee, M. Rodriguez, M. Lönnfors, M. Eisenberg-Bord, Z. Wang, S.M. Lam, M. Schuldiner, V.A. Bankaitis; Visualization: Y. Wang, P. Yuan, A. Tripathi, M. Rodriguez, M. Lönnfors, M. Eisenberg-Bord, M. Schuldiner, V.A. Bankaitis; Writing – Original Draft: Y. Wang, V.A. Bankaitis; Writing – Review and editing Y. Wang, P. Yuan, A. Tripathi, M. Lönnfors, M. Eisenberg-Bord, Z. Wang, S.M. Lam, M. Schuldiner, V.A. Bankaitis: Supervision: Y. Wang, P. Yuan, A. Tripathi, M. Lönnfors, S.M. Lam, M. Schuldiner, V.A. Bankaitis; Funding Acquisition: M. Schuldiner, V.A. Bankaitis.

Submitted: 17 July 2019
Revised: 20 December 2019
Accepted: 10 February 2020

References

Audhya, A., and S.D. Emr. 2002. Stt4 PI 4-kinase localizes to the plasma membrane and functions in the Pkc1-mediated MAP kinase cascade. *Dev. Cell.* 2:593–605. https://doi.org/10.1016/S1534-5807(02)00168-5

Baird, D., C. Stefan, A. Audhya, S. Weys, and S.D. Emr. 2008. Assembly of the PtdIns 4-kinase Stt4 complex at the plasma membrane requires Ypp1 and Efr3. *J. Cell Biol.* 183:1061–1074. https://doi.org/10.1083/jcb.200804003

Bankaitis, V.A., J.R. Aitken, A.E. Cleves, and W. Dowhan. 1990. An essential role for a phospholipid transfer protein in yeast Golgi function. *Nature.* 347:561–562. https://doi.org/10.1038/347561a0

Bankaitis, V.A., D.E. Malehorn, S.D. Emr, and R. Greene. 1989. The Saccharomyces cerevisiae SEC14 gene encodes a cytosolic factor that is required for transport of secretory proteins from the yeast Golgi complex. *J. Cell Biol.* 108:1271–1281. https://doi.org/10.1083/jcb.108.4.1271

Bankaitis, V.A., C.J. Mousley, and G. Schaaf. 2010. The Sec14 superfamily and mechanisms for crosstalk between lipid metabolism and lipid signaling. *Trends Biochem. Sci.* 35:150–160. https://doi.org/10.1016/j.tibs.2009.10.008

Baskin, J.M., X. Wu, R. Christiano, M.S. Oh, C.M. Schauder, E. Gazzerro, M. Messa, S. Baldassari, S. Assereto, R. Biancheri, et al. 2016. The leukodystrophy protein FAM126A (hyccin) regulates PtdIns(4)P synthesis at the plasma membrane. *Nat. Cell Biol.* 18:132–138. https://doi.org/10.1038/ncb3271

Boumann, H.A., J. Gubbens, M.C. Koorengevel, C.S. Oh, C.E. Martin, A.J. Heck, J. Patton-Vogt, S.A. Henry, B. de Kruijff, and A.I. de Kroon. 2006. Depletion of phosphatidylcholine in yeast induces shortening and increased saturation of the lipid acyl chains: evidence for regulation of intrinsic membrane curvature in a eukaryote. *Mol. Biol. Cell.* 17:1006–1017. https://doi.org/10.1091/mbc.e05-04-0344

Chung, J., F. Nakatsu, J.M. Baskin, and P. De Camilli. 2015a. Plasticity of PI4KIIIα interactions at the plasma membrane. *EMBO Rep.* 16:312–320. https://doi.org/10.15252/embr.201439151

Chung, J., F. Torta, K. Masai, L. Lucast, H. Czapla, L.B. Tanner, P. Narayanaswamy, M.R. Wenk, F. Nakatsu, and P. De Camilli. 2015b. PI4P/phosphatidylserine countertransport at ORP5- and ORP8-mediated ER-plasma membrane contacts. *Science.* 349:428–432. https://doi.org/10.1126/science.aab1370

Clancey, C.J., S.C. Chang, and W. Dowhan. 1993. Cloning of a gene (PSD1) encoding phosphatidylserine decarboxylase from Saccharomyces cerevisiae by complementation of an Escherichia coli mutant. *J. Biol. Chem.* 268:24580–24590.

Cleves, A.E., P.J. Novick, and V.A. Bankaitis. 1989. Mutations in the SAC1 gene suppress defects in yeast Golgi and yeast actin function. *J. Cell Biol.* 109:2939–2950. https://doi.org/10.1083/jcb.109.6.2939

De, M., A.N. Oleskie, M. Ayyash, S. Dutta, L. Mancour, M.E. Abazeed, E.J. Brace, G. Skiniotis, and R.S. Fuller. 2017. The Vps13p-Cdc31p complex is directly required for TGN late endosome transport and TGN homotypic fusion. *J. Cell Biol.* 216:425–439. https://doi.org/10.1083/jcb.201606078

Eisenberg-Bord, M., M. Mari, U. Weill, E. Rosenfeld-Gur, O. Moldavski, I.G. Castro, K.G. Soni, N. Harpaz, T.P. Levine, A.H. Futerman, et al. 2018. Identification of seipin-linked factors that act as determinants of a lipid droplet subpopulation. *J. Cell Biol.* 217:269–282. https://doi.org/10.1083/jcb.201704122

Elbaz-Alon, Y., M. Eisenberg-Bord, V. Shinder, S.B. Stiller, E. Shimoni, N. Wiedemann, T. Geiger, and M. Schuldiner. 2015. Lam6 Regulates the Extent of Contacts between Organelles. *Cell Rep.* 12:7–14. https://doi.org/10.1016/j.celrep.2015.06.022

Fang, M., B.G. Kearns, A. Gedvilaite, S. Kagiwada, M. Kearns, M.K. Fung, and V.A. Bankaitis. 1996. Kes1p shares homology with human oxysterol binding protein and participates in a novel regulatory pathway for yeast Golgi-derived transport vesicle biogenesis. *EMBO J.* 15:6447–6459. https://doi.org/10.1002/j.1460-2075.1996.tb01036.x

Foti, M., A. Audhya, and S.D. Emr. 2001. Sac1 lipid phosphatase and Stt4 phosphatidylinositol 4-kinase regulate a pool of phosphatidylinositol 4-phosphate that functions in the control of the actin cytoskeleton and vacuole morphology. *Mol. Biol. Cell.* 12:2396–2411. https://doi.org/10.1091/mbc.12.8.2396

Friedman, J.R., M. Kannan, A. Toulmay, C.H. Jan, J.S. Weissman, W.A. Prinz, and J. Nunnari. 2018. Lipid Homeostasis Is Maintained by Dual Targeting of the Mitochondrial PE Biosynthesis Enzyme to the ER. *Dev. Cell.* 44:261–270.e266.

Gatta, A.T., L.H. Wong, Y.Y. Sere, D.M. Calderón-Noreña, S. Cockcroft, A.K. Menon, and T.P. Levine. 2015. A new family of StART domain proteins at membrane contact sites has a role in ER-PM sterol transport. *eLife.* 4: e07253. https://doi.org/10.7554/eLife.07253

Grabon, A., A. Orłowski, A. Tripathi, J. Vuorio, M. Javanainen, T. Róg, M. Lönnfors, M.I. McDermott, G. Siebert, P. Somerharju, et al. 2017. Dynamics and energetics of the mammalian phosphatidylinositol transfer protein phospholipid exchange cycle. *J. Biol. Chem.* 292:14438–14455. https://doi.org/10.1074/jbc.M117.791467

Graham, T.R., and C.G. Burd. 2011. Coordination of Golgi functions by phosphatidylinositol 4-kinases. *Trends Cell Biol.* 21:113–121. https://doi.org/10.1016/j.tcb.2010.10.002

Gulshan, K., P. Shahi, and W.S. Moye-Rowley. 2010. Compartment-specific synthesis of phosphatidylethanolamine is required for normal heavy metal resistance. *Mol. Biol. Cell.* 21:443–455. https://doi.org/10.1091/mbc.e09-06-0519

Guo, S., L.E. Stolz, S.M. Lemrow, and J.D. York. 1999. SAC1-like domains of yeast SAC1, INP52, and INP53 and of human synaptojanin encode polyphosphoinositide phosphatases. *J. Biol. Chem.* 274:12990–12995. https://doi.org/10.1074/jbc.274.19.12990

Huang, J., R. Ghosh, A. Tripathi, M. Lönnfors, P. Somerharju, and V.A. Bankaitis. 2016. Two-ligand priming mechanism for potentiated phosphoinositide synthesis is an evolutionarily conserved feature of Sec14-like phosphatidylinositol and phosphatidylcholine exchange proteins. *Mol. Biol. Cell.* 27:2317–2330. https://doi.org/10.1091/mbc.E16-04-0221

Huang, J., C.J. Mousley, L. Dacquay, N. Maitra, G. Drin, C. He, N.D. Ridgway, A. Tripathi, M. Kennedy, B.K. Kennedy, et al. 2018. A Lipid Transfer Protein Signaling Axis Exerts Dual Control of Cell-Cycle and Membrane Trafficking Systems. *Dev. Cell.* 44:378–391.e375.

Ile, K.E., S. Kassen, C. Cao, T. Vihtehlic, S.D. Shah, C.J. Mousley, J.G. Alb Jr., R.P. Huijbregts, G.W. Stearns, S.E. Brockerhoff, et al. 2010. Zebrafish class 1 phosphatidylinositol transfer proteins: PITPbeta and double cone cell outer segment integrity in retina. *Traffic.* 11:1151–1167. https://doi.org/10.1111/j.1600-0854.2010.01085.x

Kanehara, K., C.Y. Yu, Y. Cho, W.F. Cheong, F. Torta, G. Shui, M.R. Wenk, and Y. Nakamura. 2015. Arabidopsis AtPLC2 Is a Primary Phosphoinositide-Specific Phospholipase C in Phosphoinositide Metabolism and the Endoplasmic Reticulum Stress Response. *PLoS Genet.* 11:e1005511. https://doi.org/10.1371/journal.pgen.1005511

Kumar, N., M. Leonzino, W. Hancock-Cerutti, F.A. Horenkamp, P. Li, J.A. Lees, H. Wheeler, K.M. Reinisch, and P. De Camilli. 2018. VPS13A and VPS13C are lipid transport proteins differentially localized at ER contact sites. *J. Cell Biol.* 217:3625–3639. https://doi.org/10.1083/jcb.201807019

Levine, T., and C. Loewen. 2006. Inter-organelle membrane contact sites: through a glass, darkly. *Curr. Opin. Cell Biol.* 18:371–378. https://doi.org/10.1016/j.ceb.2006.06.011

Li, X., M.P. Rivas, M. Fang, J. Marchena, B. Mehrotra, A. Chaudhary, L. Feng, G.D. Prestwich, and V.A. Bankaitis. 2002. Analysis of oxysterol binding protein homologue Kes1p function in regulation of Sec14p-dependent protein transport from the yeast Golgi complex. *J. Cell Biol.* 157:63–77. https://doi.org/10.1083/jcb.200201037

Lu, J., S.M. Lam, Q. Wan, L. Shi, Y. Huo, L. Chen, X. Tang, B. Li, X. Wu, K. Peng, et al. 2019. High-Coverage Targeted Lipidomics Reveals Novel Serum Lipid Predictors and Lipid Pathway Dysregulation Antecedent to Type 2 Diabetes Onset in Normoglycemic Chinese Adults. *Diabetes Care.* 42:2117–2126. https://doi.org/10.2337/dc19-0100

Manford, A.G., C.J. Stefan, H.L. Yuan, J.A. Macgurn, and S.D. Emr. 2012. ER-to-plasma membrane tethering proteins regulate cell signaling and ER morphology. *Dev. Cell.* 23:1129–1140. https://doi.org/10.1016/j.devcel.2012.11.004

Moser von Filseck, J., A. Čopič, V. Delfosse, S. Vanni, C.L. Jackson, W. Bourguet, and G. Drin. 2015. Phosphatidylserine transport by ORP/Osh proteins is driven by phosphatidylinositol 4-phosphate. *Science.* 349: 432–436. https://doi.org/10.1126/science.aab1346

Murley, A., R.D. Sarsam, A. Toulmay, J. Yamada, W.A. Prinz, and J. Nunnari. 2015. Ltc1 is an ER-localized sterol transporter and a component of ER-mitochondria and ER-vacuole contacts. *J. Cell Biol.* 209:539–548. https://doi.org/10.1083/jcb.201502033

Nakatsu, F., J.M. Baskin, J. Chung, L.B. Tanner, G. Shui, S.Y. Lee, M. Pirruccello, M. Hao, N.T. Ingolia, M.R. Wenk, and P. De Camilli. 2012. PtdIns4P synthesis by PI4KIIIα at the plasma membrane and its impact on plasma membrane identity. *J. Cell Biol.* 199:1003–1016. https://doi.org/10.1083/jcb.201206095

Nemoto, Y., B.G. Kearns, M.R. Wenk, H. Chen, K. Mori, J.G. Alb Jr., P. De Camilli, and V.A. Bankaitis. 2000. Functional characterization of a mammalian Sac1 and mutants exhibiting substrate-specific defects in phosphoinositide phosphatase activity. *J. Biol. Chem.* 275:34293–34305. https://doi.org/10.1074/jbc.M003923200

Nile, A.H., A. Tripathi, P. Yuan, C.J. Mousley, S. Suresh, I.M. Wallace, S.D. Shah, D.T. Pohlhaus, B. Temple, C. Nislow, et al. 2014. PITPs as targets for selectively interfering with phosphoinositide signaling in cells. *Nat. Chem. Biol.* 10:76–84. https://doi.org/10.1038/nchembio.1389

Phillips, S.E., B. Sha, L. Topalof, Z. Xie, J.G. Alb, V.A. Klenchin, P. Swigart, S. Cockcroft, T.F. Martin, M. Luo, and V.A. Bankaitis. 1999. Yeast Sec14p deficient in phosphatidylinositol transfer activity is functional in vivo. *Mol. Cell.* 4:187–197. https://doi.org/10.1016/S1097-2765(00)80366-4

Quon, E., Y.Y. Sere, N. Chauhan, J. Johansen, D.P. Sullivan, J.S. Dittman, W.J. Rice, R.B. Chan, G. Di Paolo, C.T. Beh, and A.K. Menon. 2018. Endoplasmic reticulum-plasma membrane contact sites integrate sterol and phospholipid regulation. *PLoS Biol.* 16:e2003864. https://doi.org/10.1371/journal.pbio.2003864

Raychaudhuri, S., and W.A. Prinz. 2010. The diverse functions of oxysterol-binding proteins. *Annu. Rev. Cell Dev. Biol.* 26:157–177. https://doi.org/10.1146/annurev.cellbio.042308.113334

Ren, J., C. Pei-Chen Lin, M.C. Pathak, B.R. Temple, A.H. Nile, C.J. Mousley, M.C. Duncan, D.M. Eckert, T.J. Leiker, P.T. Ivanova, et al. 2014. A phosphatidylinositol transfer protein integrates phosphoinositide signaling with lipid droplet metabolism to regulate a developmental program of nutrient stress-induced membrane biogenesis. *Mol. Biol. Cell.* 25:712–727. https://doi.org/10.1091/mbc.e13-11-0634

Riekhof, W.R., W.I. Wu, J.L. Jones, M. Nikrad, M.M. Chan, C.J. Loewen, and D.R. Voelker. 2014. An assembly of proteins and lipid domains regulates transport of phosphatidylserine to phosphatidylserine decarboxylase 2 in Saccharomyces cerevisiae. *J. Biol. Chem.* 289:5809–5819. https://doi.org/10.1074/jbc.M113.518217

Rivas, M.P., B.G. Kearns, Z. Xie, S. Guo, M.C. Sekar, K. Hosaka, S. Kagiwada, J.D. York, and V.A. Bankaitis. 1999. Pleiotropic alterations in lipid metabolism in yeast sac1 mutants: relationship to "bypass Sec14p" and inositol auxotrophy. *Mol. Biol. Cell.* 10:2235–2250. https://doi.org/10.1091/mbc.10.7.2235

Roy, A., and T.P. Levine. 2004. Multiple pools of phosphatidylinositol 4-phosphate detected using the pleckstrin homology domain of Osh2p. *J. Biol. Chem.* 279:44683–44689. https://doi.org/10.1074/jbc.M401583200

Schaaf, G., E.A. Ortlund, K.R. Tyeryar, C.J. Mousley, K.E. Ile, T.A. Garrett, J. Ren, M.J. Woolls, C.R. Raetz, M.R. Redinbo, and V.A. Bankaitis. 2008. Functional anatomy of phospholipid binding and regulation of phosphoinositide homeostasis by proteins of the sec14 superfamily. *Mol. Cell.* 29:191–206. https://doi.org/10.1016/j.molcel.2007.11.026

Scorrano, L., M.A. De Matteis, S. Emr, F. Giordano, G. Hajnóczky, B. Kornmann, L.L. Lackner, T.P. Levine, L. Pellegrini, K. Reinisch, et al. 2019. Coming together to define membrane contact sites. *Nat. Commun.* 10: 1287. https://doi.org/10.1038/s41467-019-09253-3

Sha, B., S.E. Phillips, V.A. Bankaitis, and M. Luo. 1998. Crystal structure of the Saccharomyces cerevisiae phosphatidylinositol-transfer protein. *Nature.* 391:506–510. https://doi.org/10.1038/35179

Shai, N., E. Yifrach, C.W.T. van Roermund, N. Cohen, C. Bibi, I.J. Lodewijk, L. Cavellini, J. Meurisse, R. Schuster, L. Zada, et al. 2018. Systematic mapping of contact sites reveals tethers and a function for the peroxisome-mitochondria contact. *Nat. Commun.* 9:1761.

Somerharju, P.J., D. van Loon, and K.W. Wirtz. 1987. Determination of the acyl chain specificity of the bovine liver phosphatidylcholine transfer protein. Application of pyrene-labeled phosphatidylcholine species. *Biochemistry.* 26:7193–7199. https://doi.org/10.1021/bi00396a048

Stefan, C.J., A. Audhya, and S.D. Emr. 2002. The yeast synaptojanin-like proteins control the cellular distribution of phosphatidylinositol (4,5)-bisphosphate. *Mol. Biol. Cell.* 13:542–557. https://doi.org/10.1091/mbc.01-10-0476

Stefan, C.J., A.G. Manford, D. Baird, J. Yamada-Hanff, Y. Mao, and S.D. Emr. 2011. Osh proteins regulate phosphoinositide metabolism at ER-plasma membrane contact sites. *Cell.* 144:389–401. https://doi.org/10.1016/j.cell.2010.12.034

Storey, M.K., K.L. Clay, T. Kutateladze, R.C. Murphy, M. Overduin, and D.R. Voelker. 2001. Phosphatidylethanolamine has an essential role in Saccharomyces cerevisiae that is independent of its ability to form hexagonal phase structures. *J. Biol. Chem.* 276:48539–48548. https://doi.org/10.1074/jbc.M109043200

Strahl, T., H. Hama, D.B. DeWald, and J. Thorner. 2005. Yeast phosphatidylinositol 4-kinase, Pik1, has essential roles at the Golgi and in the nucleus. *J. Cell Biol.* 171:967–979. https://doi.org/10.1083/jcb.200504104

Tani, M., and O. Kuge. 2014. Involvement of Sac1 phosphoinositide phosphatase in the metabolism of phosphatidylserine in the yeast Saccharomyces cerevisiae. *Yeast.* 31:145–158. https://doi.org/10.1002/yea.3004

Teixeira, V., L. Johnsen, F. Martínez-Montañés, A. Grippa, L. Buxó, F.Z. Idrissi, C.S. Ejsing, and P. Carvalho. 2018. Regulation of lipid droplets by metabolically controlled Ldo isoforms. *J. Cell Biol.* 217:127–138. https://doi.org/10.1083/jcb.201704115

Tian, S., A. Ohta, H. Horiuchi, and R. Fukuda. 2018. Oxysterol-binding protein homologs mediate sterol transport from the endoplasmic reticulum to mitochondria in yeast. *J. Biol. Chem.* 293:5636–5648. https://doi.org/10.1074/jbc.RA117.000596

Tripathi, A., E. Martinez, A.J. Obaidullah, M.G. Lete, M. Lönnfors, D. Khan, K.G. Soni, C.J. Mousley, G.E. Kellogg, and V.A. Bankaitis. 2019. Functional diversification of the chemical landscapes of yeast Sec14-like phosphatidylinositol transfer protein lipid-binding cavities. *J. Biol. Chem.* 294:19081–19098. https://doi.org/10.1074/jbc.RA119.011153

Trotter, P.J., and D.R. Voelker. 1995. Identification of a non-mitochondrial phosphatidylserine decarboxylase activity (PSD2) in the yeast Saccharomyces cerevisiae. *J. Biol. Chem.* 270:6062–6070. https://doi.org/10.1074/jbc.270.11.6062

Trotter, P.J., J. Pedretti, and D.R. Voelker. 1993. Phosphatidylserine decarboxylase from Saccharomyces cerevisiae. Isolation of mutants, cloning of the gene, and creation of a null allele. *J. Biol. Chem.* 268: 21416–21424.

Trotter, P.J., W.I. Wu, J. Pedretti, R. Yates, and D.R. Voelker. 1998. A genetic screen for aminophospholipid transport mutants identifies the phosphatidylinositol 4-kinase, STT4p, as an essential component in phosphatidylserine metabolism. *J. Biol. Chem.* 273:13189–13196. https://doi.org/10.1074/jbc.273.21.13189

Valm, A.M., S. Cohen, W.R. Legant, J. Melunis, U. Hershberg, E. Wait, A.R. Cohen, M.W. Davidson, E. Betzig, and J. Lippincott-Schwartz. 2017. Applying systems-level spectral imaging and analysis to reveal the organelle interactome. *Nature.* 546:162–167. https://doi.org/10.1038/nature22369

Voelker, D.R. 2005. Bridging gaps in phospholipid transport. *Trends Biochem. Sci.* 30:396–404. https://doi.org/10.1016/j.tibs.2005.05.008

Wang, Y., C.J. Mousley, M.G. Lete, and V.A. Bankaitis. 2019. An equal opportunity collaboration between lipid metabolism and proteins in the control of membrane trafficking in the trans-Golgi and endosomal systems. *Curr. Opin. Cell Biol.* 59:58–72. https://doi.org/10.1016/j.ceb.2019.03.012

Wu, H., P. Carvalho, and G.K. Voeltz. 2018. Here, there, and everywhere: The importance of ER membrane contact sites. *Science.* 361:eaan5835. https://doi.org/10.1126/science.aan5835

Wu, W.I., S. Routt, V.A. Bankaitis, and D.R. Voelker. 2000. A new gene involved in the transport-dependent metabolism of phosphatidylserine, PSTB2/PDR17, shares sequence similarity with the gene encoding the phosphatidylinositol/phosphatidylcholine transfer protein, SEC14. *J. Biol. Chem.* 275:14446–14456. https://doi.org/10.1074/jbc.275.19.14446

Xie, Z., S.K. Hur, L. Zhao, C.S. Abrams, and V.A. Bankaitis. 2018. A Golgi Lipid Signaling Pathway Controls Apical Golgi Distribution and Cell Polarity during Neurogenesis. *Dev. Cell.* 44:725–740.e724.

JCB

Supplemental material

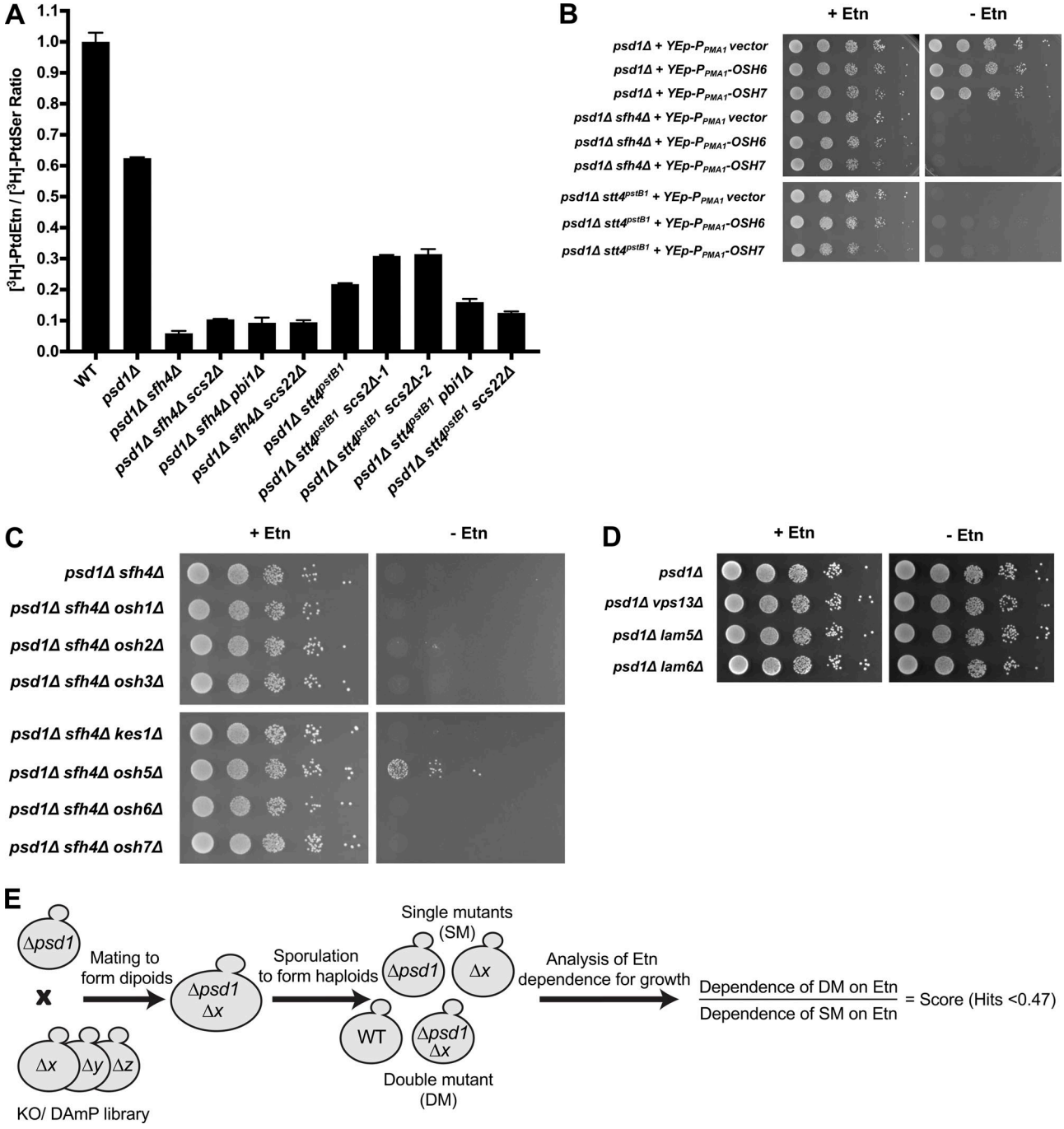

Figure S1. **Functional ablation of individual candidate MCS tethers does not influence Psd2 activity in vivo. (A)** The efficiencies of PtdSer decarboxylation to PtdEtn were measured for the indicated yeast strains by radiolabeling cells with [^{3}H]-serine, extraction of total phospholipid, and quantification of [^{3}H]-PtdSer and [^{3}H]-PtdEtn. The conversion of PtdSer to PtdEtn was expressed as the [^{3}H]-PtdEtn/[^{3}H]-PtdSer ratios of the indicated strains and related to the [^{3}H]-PtdEtn/[^{3}H]-PtdSer ratio of the WT control (set as 1.0). The *psd1Δ stt4^{pstB1} scs2Δ-1* and *psd1Δ stt4^{pstB1} scs2Δ-2* mutants are independently generated strains with the same genotype. Values represent averages from three independent experiments plotted as mean ± SEM. **(B)** Isogenic yeast strains of the designated genotype transformed with a mock YEp vector, or with YEp vectors driving *OSH6* or *OSH7* gene expression under *PMA1* promoter control, were spotted in 10-fold dilution series on uracil-free medium ± 2 mM Etn and incubated at 30°C for 72 h. **(C and D)** Isogenic yeast strains of the designated genotype were spotted in 10-fold dilution series on synthetic complete medium ± 2 mM Etn and incubated at 30°C for 72 h. **(E)** Design of the synthetic gene array screen for identifying components required for Psd2 activity in vivo. Schematic illustration of the screen aimed to find nonessential genes whose functional ablation, when combined with the *psd1Δ* allele, retards growth on Etn-free medium. A *psd1Δ* allele was recombined into the yeast gene deletion collection using a standard automated mating, sporulation and selection protocol. Colony sizes of yeast containing both the query library gene deletion and *psd1Δ* (double mutants, DM) were analyzed by relating colony sizes achieved on plates lacking Etn relative to those on Etn-replete medium. To validate that the observed growth deficit was Δ*psd1*-dependent, and not simply a result of the library background, the same analysis was performed on yeast that were only selected for the mutant allele from the library (single mutants, SM). Normalized growth deficits were calculated, and DM strains that exhibited a growth score <1 SD from the mean (<0.47) were considered potential hits.

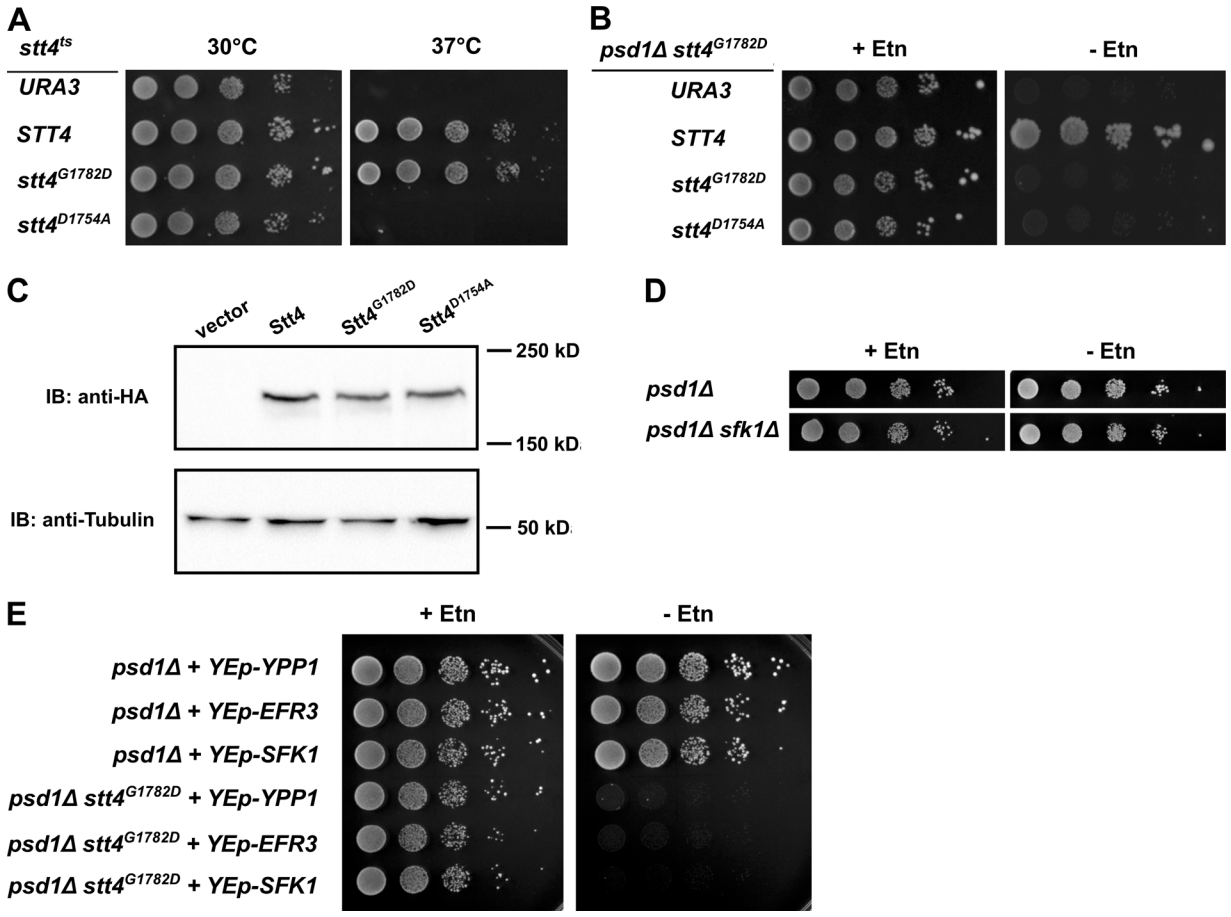

Figure S2. **Phenotypic assays of *stt4* mutants and Stt4 subunit–overexpressing cells. (A)** Isogenic *stt4*^{ts} yeast transformed with YCp(*URA3*) or derivatives driving individual expression of *STT4*, *stt4*^{G1782D}, or *stt4*^{D1754A} from the natural *STT4* promoter were spotted in 10-fold dilution series on uracil-free medium and incubated for 72 h at the permissive and restrictive temperatures of 30°C and 37°C. **(B)** Isogenic *psd1Δ stt4*^{G1782D} yeast transformed with YCp(*URA3*) or derivatives driving individual expression of *STT4*, *stt4*^{G1782D}, or *stt4*^{D1754A} genes from the natural *STT4* promoter were spotted in 10-fold dilution series on uracil-free medium ± 2 mM Etn and incubated at 30°C for 72 h. **(C)** Lysates were prepared from WT yeast transformed with *YEp(URA3)* or with *YEp(URA3)* derivatives driving individual expression of Stt4-HA, Stt4^{G1782D}-HA, or Stt4^{D1754A}-HA from the natural *STT4* promoter. Lysates from equal amount of cells were loaded. Stt4-HA and tubulin (normalization control) were visualized by immunoblotting (IB) using anti-HA or anti-tubulin antibodies, respectively. **(D)** Isogenic yeast strains of the designated genotype were spotted in 10-fold dilution series on synthetic complete medium ± 2 mM Etn and incubated at 30°C for 72 h. **(E)** Isogenic *psd1Δ* or *psd1Δ stt4*^{G1782D} yeast transformed with multicopy YEp vectors driving *YPP1*, *EFR3*, or *SFK1* overexpression (from their respective natural promoters) were spotted in 10-fold dilution series on uracil-free medium ± 2 mM Etn and incubated at 30°C for 72 h.

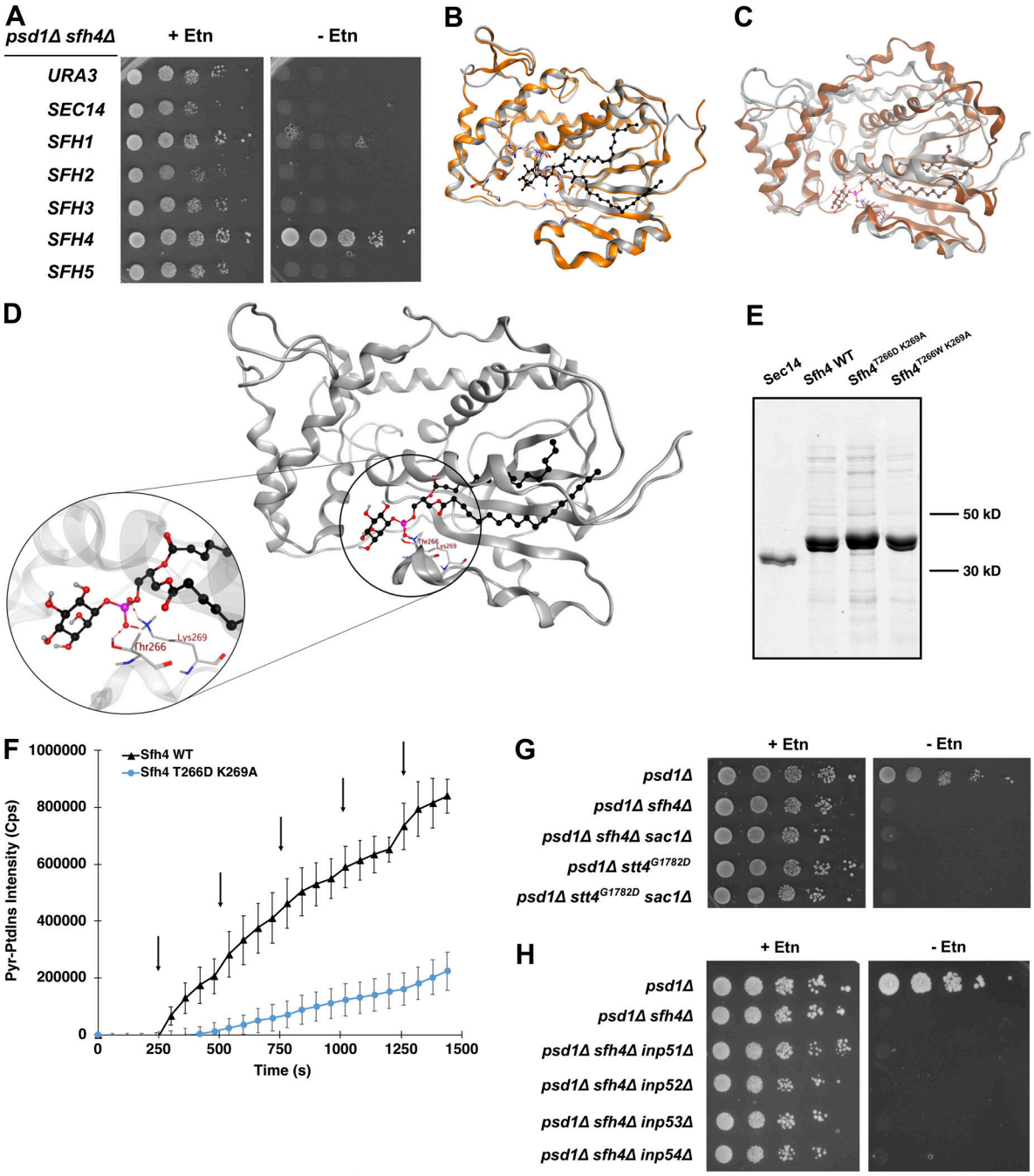

Figure S3. **Sfh4::PtdIns homology model and the PtdIns-binding motif. (A)** Isogenic *psd1Δ sfh4Δ* yeast transformed with yeast episomal *URA3* plasmids driving high levels of expression of each individual member of the yeast Sec14-like PITP family (identified at left), from the *PMA1* promoter, were spotted in a 10-fold dilution series on uracil-free selection medium with or without Etn as indicated at top. Plates were incubated at 30°C for 72 h. **(B)** Homology model of Sfh4::PtdIns complex (gray ribbon) threaded onto the Sfh3 crystal structure (PDB: 4J7Q) template (orange ribbon). **(C)** Sfh4::PtdIns homology model (gray ribbon) is superimposed onto the Sfh1 structure (PDB: 3B7N, brown ribbon). Figure shows conservation of structural fold and of the PtdIns binding pose. **(D)** Homology model of the Sfh4::PtdIns complex is rendered as gray ribbon. Enlarged panel highlights the conserved Sec14-like PITP PtdIns headgroup coordination motif, and illustrate conserved residues T_{266} and K_{269} interacting with PtdIns headgroup phosphate via a network of H-bonds. **(E)** Coomassie-stained SDS-PAGE gel of purified recombinant Sec14, Sfh4, $Sfh4^{T266D,K269A}$, and $Sfh4^{T266W,K269A}$ proteins used in this study. **(F)** Fluorescence dequenching PtdIns-transfer assay for purified recombinant Sfh4 and $Sfh4^{T266D,K269A}$. Fluorescence intensity of pyrene-PtdIns is plotted as a function of time. Black arrows identify points at which a 1-μg increment of the indicated protein was added. After protein addition, the observed increase in fluorescence intensity is directly proportional to the relative transfer efficiency of the protein being assayed. Values represent averages from two independent experiments plotted as mean ± SD. **(G)** Yeast growth assay showing that *sac1Δ* failed to restore Psd2 pathway activity in mutants ablated for Sfh4 function and compromised for Stt4 activity. Isogenic yeast strains were spotted in 10-fold dilution series on glucose minimal agar plates ± 2 mM Etn, as indicated, and incubated at 30°C for 72 h. **(H)** Yeast growth assay showing the *inp51Δ*, *inp52Δ*, *inp53Δ*, and *inp54Δ* alleles that inactivate distinct phosphoinositide phosphatases strain failed to rescue Psd2 activity in *psd1Δ sfh4Δ* cells. Isogenic yeast strains with the designated genotype were spotted in 10-fold dilution series on glucose minimal agar plates ± 2 mM Etn, as indicated, and incubated at 30°C for 72 h.

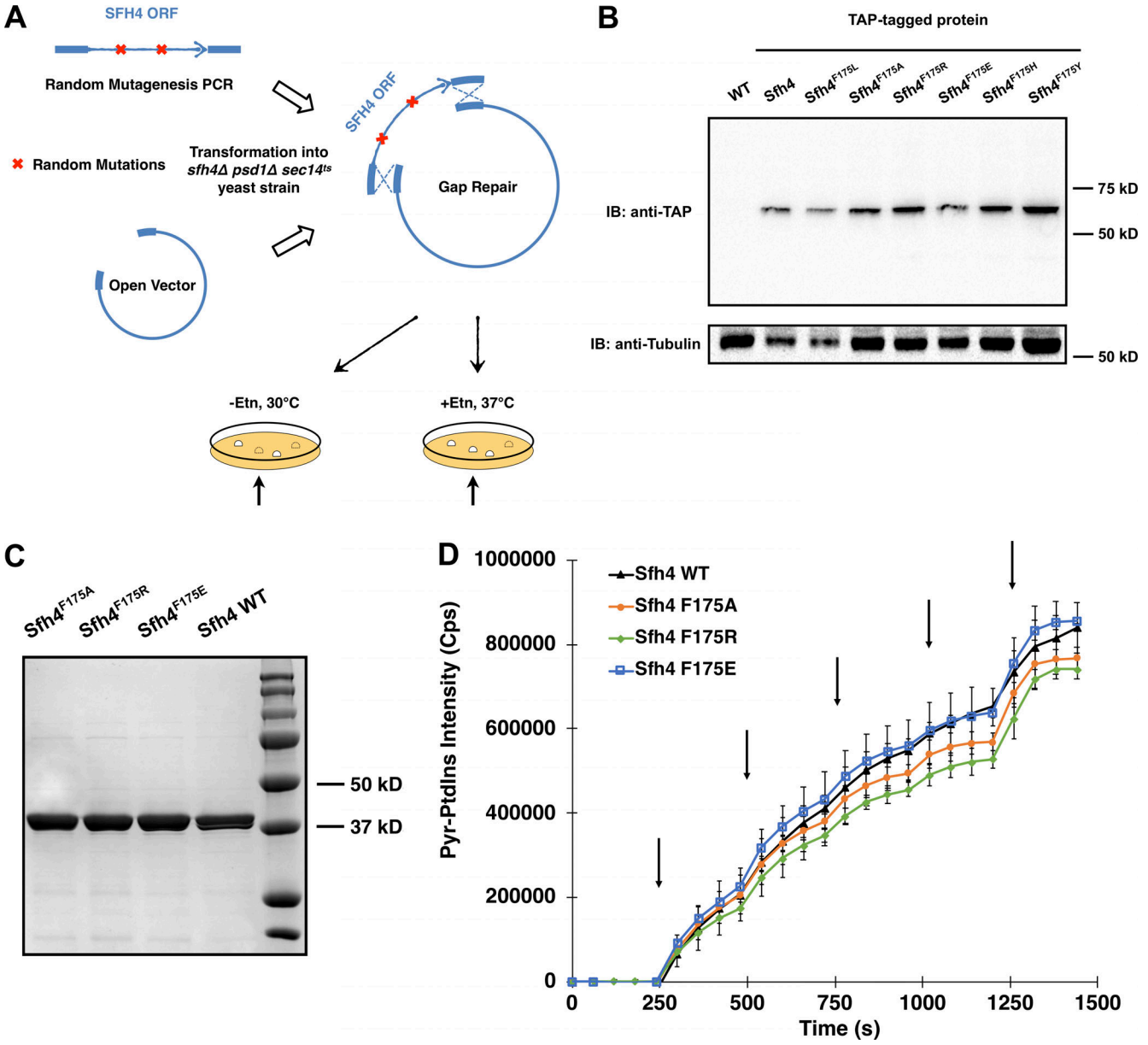

Figure S4. **The mutagenic PCR screen and the fluorescence dequenching PtdIns-transfer assay of *sfh4* mutants. (A)** Design of the mutagenic PCR screen for isolation of Sfh4 mutants specifically defective in Psd2 activity. A PCR-mutagenized *SFH4* fragment library was cotransformed with a gapped YCp(*URA3*) plasmid into the *ura3 sfh4Δ psd1Δ sec14*^{ts} recipient strain. Transformants displaying the unselected parental Etn auxotrophy and the ability to grow at 37°C were identified. **(B)** Lysates were prepared from WT yeast strains or WT yeast expressing TAP-tagged Sfh4 proteins from the endogenous genomic locus. Loading was normalized by cell number. Sfh4-TAP and tubulin (normalization control) were visualized by immunoblotting (IB) with anti-TAP or anti-tubulin antibodies, respectively. **(C)** Coomassie-stained SDS-PAGE gel of purified recombinant Sfh4 WT, Sfh4^{F175A}, Sfh4^{F175R}, and Sfh4^{F175E} proteins used in this study. **(D)** Fluorescence dequenching PtdIns-transfer assay for purified recombinant Sfh4, Sfh4^{F175A}, Sfh4^{F175R}, and Sfh4^{F175E} proteins. Fluorescence intensity of pyrene-PtdIns is plotted as a function of time. Black arrows identify points at which a 1-µg increment of the indicated protein was added. After protein addition, the observed increase in fluorescence intensity is directly proportional to the relative transfer efficiency of the protein being assayed. Values represent averages from two independent experiments plotted as mean ± SD. These mutant Sfh4 data were obtained in the same experiments as the data reported in Fig. S3 F, so the same Sfh4 control data are represented in both figures.

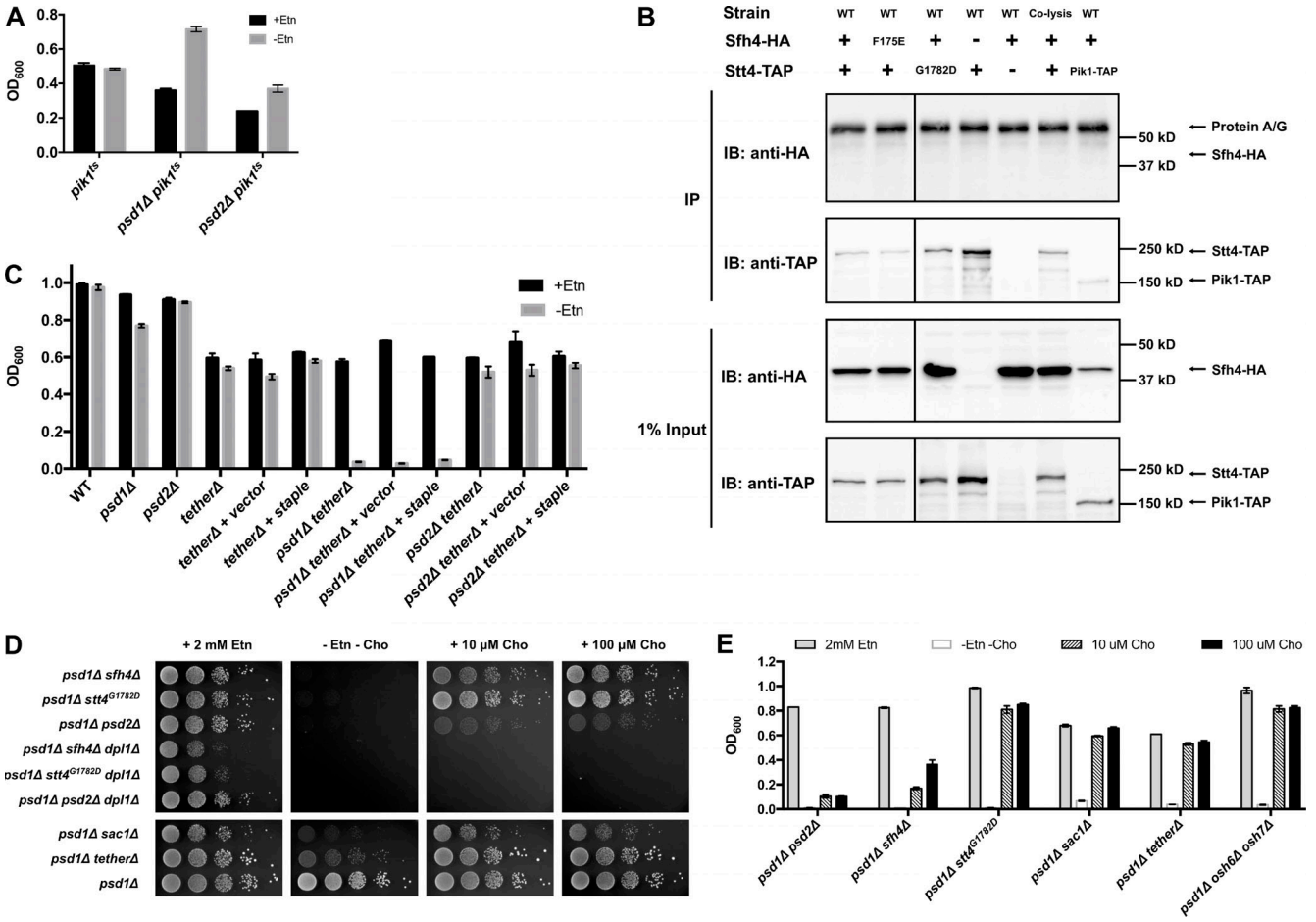

Figure S5. **Stt4-dependent PtdIns4*P* homeostasis regulates Psd2 activity indirectly. (A)** Growth of the indicated yeast strains in glucose minimal liquid medium with or without supplementation with Etn (2 mM). The assays were otherwise conducted as described in Fig. 4 B. Cultures were grown at 30°C for 46.5 h (PtdIns4*P* synthesis in the *pik1*^{ts} strain is significantly compromised even at 26°C; Li et al., 2002), and the final A_{600} of each culture was recorded. Values represent averages of two independent experiments (n = 2) plotted as mean ± range. **(B)** WT yeast cells with *STT4-TAP*, *stt4*^{G1782D}*-TAP*, or *PIK1-TAP* cassettes transplaced for the endogenous genes were transformed with a yeast episomal plasmid driving expression of Sfh4-HA under *SFH4* promoter control and cultured to midlogarithmic growth phase, and cell-free lysates were prepared. The coimmunoprecipitation (coIP) experiment was performed as described in the legend to Fig. 5 A. The left and right sections of the figure were from the same blot. IB, immunoblotting. **(C)** Growth of the indicated yeast strains in glucose minimal liquid medium with or without Etn (2 mM) as indicated. The assay was otherwise conducted as described in Fig. 4 B. Cultures were grown at 30°C for 46.5 h, and the final A_{600} of each culture was recorded. Staple refers to expression of the artificial ER-PM tether. Values represent averages of two independent experiments (n = 2) plotted as mean ± range. **(D)** Isogenic yeast strains with the designated genotype were spotted in 10-fold dilution series on synthetic complete medium + 2 mM Etn, +10 µM choline, +100 µM choline or without Etn or choline and incubated at 30°C for 72 h. **(E)** Growth of the indicated yeast strains in glucose minimal liquid medium without Etn or choline supplementation (open bars), or supplemented with 2 mM Etn (gray bars), 10 µM choline (filled bars), and 100 µM choline (black bars). The assay was otherwise conducted as described in Fig. 4 B. Cultures were grown at 30°C for 46.5 h, and the final A_{600} of each culture was recorded. Values represent averages of two independent experiments (n = 2) plotted as mean ± range.

Provided online are four tables. Table S1 shows a synthetic genetic array screen interrogating yeast genome for the loss of function of any of yeast nonessential genes that deactivate the Psd2 pathway. Table S2 lists the genotypes of yeast strains used in this study. Table S3 lists the plasmids used in this study. Table S4 lists the primers used in this study.